International Journal of Biological Macromolecules 261 (2024) 129712

Contents lists available at ScienceDirect

International Journal of Biological Macromolecules

journal homepage: www.elsevier.com/locate/ijbiomac

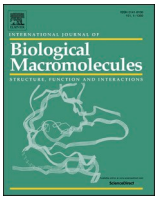

# Molecular dynamics simulations reveal the parallel stranded d(GGGA)$_3$GGG DNA quadruplex folds via multiple paths from a coil-like ensemble

Pavlína Pokorná [a,1], Vojtěch Mlýnský [a], Giovanni Bussi [b], Jiří Šponer [a], Petr Stadlbauer [a,*]

[a] Institute of Biophysics of the Czech Academy of Sciences, Královopolská 135, Brno 61200, Czech Republic
[b] Scuola Internazionale Superiore di Studi Avanzati (SISSA), via Bonomea 265, Trieste 34136, Italy

ARTICLE INFO

*Keywords:*
G-Quadruplex
Folding
Molecular dynamics

ABSTRACT

G-quadruplexes (G4s) are non-canonical nucleic acid structures that fold through complex processes. Characterization of the G4 folding landscape may help to elucidate biological roles of G4s but is challenging both experimentally and computationally. Here, we achieved complete folding of a three-quartet parallel DNA G4 with (GGGA)$_3$GGG sequence using all-atom explicit-solvent enhanced-sampling molecular dynamics (MD) simulations. The simulations suggested early formation of guanine stacks in the G-tracts, which behave as semi-rigid blocks in the folding process. The folding continues via the formation of a collapsed compact coil-like ensemble. Structuring of the G4 from the coil then proceeds via various cross-like, hairpin, slip-stranded and two-quartet ensembles and can bypass the G-triplex structure. Folding of the parallel G4 does not appear to involve any salient intermediates and is a multi-pathway process. We also carried out an extended set of simulations of parallel G-hairpins. While parallel G-hairpins are extremely unstable when isolated, they are more stable inside the coil structure. On the methodology side, we show that the AMBER DNA force field predicts the folded G4 to be less stable than the unfolded ensemble, uncovering substantial force-field issues. Overall, we provide unique atomistic insights into the folding landscape of parallel-stranded G4 but also reveal limitations of current state-of-the-art MD techniques.

## 1. Introduction

G-quadruplexes (G4s) are non-canonical nucleic acid structures formed by guanine-rich sequences. Localized predominantly in telomeres and gene regulatory regions, they may be involved in genome replication and maintenance, gene expression control and the development of diseases such as cancer [1–3]. Besides their biological roles and therapeutic targeting potential, they have applications in nanotechnology [4,5].

The core of the G4 structure is formed by four guanine bases H-bonded together in a planar arrangement, i.e., a quartet (Fig. 1). Some DNA G4s are structurally polymorphic and can adopt several different folds with diverse orientations of their G-strands and the connecting loops [6–8]. Different folds formed by the same sequence differ in their stabilities depending on the environmental conditions, such as salt conditions or protein binding [9]. The *syn* (*s*) and *anti* (*a*) orientations of individual guanine glycosidic torsion angles are the basis for the *syn-anti* pattern of the whole G4. However, not all *syn-anti* patterns can form a G4; the basic rule is that if two G-strands run parallel to each other, their two guanines participating in the same quartet must both have the same glycosidic orientation. In contrast, for antiparallel G-strands, two guanines in a given quartet have opposite glycosidic orientations (Fig. 1) [10]. Additionally, a single-nucleotide loop predominantly folds into a propeller topology, and thus only supports a parallel G-strand orientation [11–13].

Overall, G4 folding is a complex multi-pathway process where equilibrium is often reached slowly. In vitro experiments have revealed folding times ranging from sub-seconds up to many hours, going far beyond timescales relevant to many cellular processes [14–16]. In addition, both excessive stabilization and destabilization of G4s have

* Corresponding author.
*E-mail address:* stadlbauer@ibp.cz (P. Stadlbauer).
[1] Present address: Pavlína Pokorná, National Research Council of Italy (CNR)-IOM c/o Scuola Internazionale Superiore di Studi Avanzati (SISSA), via Bonomea 265, Trieste 34,136, Italy.

https://doi.org/10.1016/j.ijbiomac.2024.129712
Received 21 September 2023; Received in revised form 10 January 2024; Accepted 16 January 2024
Available online 28 January 2024

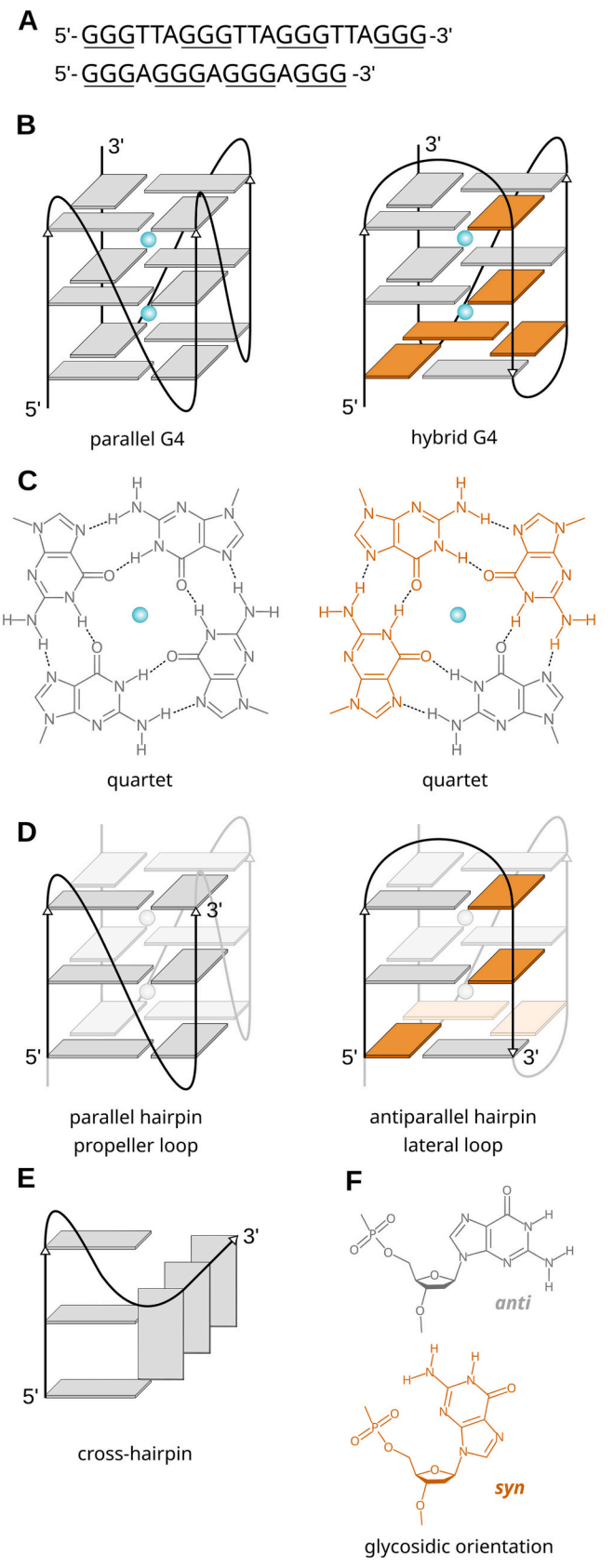


*(caption on next column)*

**Fig. 1.** Examples of G4 topologies. (A) Examples of G4-forming sequences, G-tracts are underlined. (B) Schemes of three-quartet parallel and hybrid G4s, bases in *anti* conformation are in gray, *syn* in orange, and the blue spheres represent cations. (C) Structural formulas of the bottom quartets of G4s from (B), H-bonds are marked with dashed lines. (D) Hairpins derived from parallel and hybrid G4s. The propeller loop is also called the double-chain-reversal loop. (E) Scheme of a cross-hairpin structure. The G-tracts are perpendicular to each other. (F) *Anti* and *syn* guanosine orientations. (For interpretation of the references to colour in this figure legend, the reader is referred to the web version of this article.)

been reported to have pathological consequences, suggesting that the balance of folding-unfolding kinetics is important for G4 regulatory functions [17]. Thus, not only are the equilibrium ensembles and significant local minima G4 structures expected to be biologically relevant but also the pathways and kinetics of G4 folding and transitions among the folds [14,15,18].

From the folding landscape theory perspective, G4 folding can be best described by the kinetic partitioning mechanism, which is a competition between two or more long-lived species [19]. It has been suggested that the long-lived species forming the dominant free energy basins on the landscape are diverse G4 folds [19,20]. The folding landscape of a G4 may contain several competing quadruplex topologies, including G4 structures with formal strand slippage (register shift, reducing the number of G-quartets). For many sequences, competition between several G4 structures has been experimentally detected, but other undetectable G4 species may be present transiently during the folding process. Indeed, for the most widely-studied G4, the human telomeric $(GGGTTA)_n$ sequence, a multi-pathway branched folding processes involving several species with differing lifetimes has been demonstrated by NMR, circular dichroism, FRET and mass spectroscopy experiments [18,20–24]. Obviously, the folding landscape must also include transitions between the different long-lived species. Thus, besides diverse G4 topologies, a rich spectrum of structures and substates is expected to be transiently populated during individual folding events or transitions between different G4 topologies. Among them, G-hairpins, G-triplexes and cross-hairpin structures (Fig. 1) have been suggested as prominent [22,25–35]. Experimental investigations of transiently populated partially folded species are extremely challenging due to their short lifetimes, low populations and structural fluxionality. Nevertheless, these structures and ensembles are important because they can form bottlenecks for transitions between unfolded and folded states or between long-lived G4 species.

Molecular dynamics (MD) simulations are a viable tool for studying the transient ensembles and dynamic processes owing to their detailed spatial and temporal resolution. They have been used to investigate different aspects of G4s [25,28,29,32,34–49]. Standard MD simulations are often limited by the affordable sampling. Therefore, diverse enhanced sampling methods have been used. These act either generally by modifying the total energy of the system or on a specifically selected low-dimensional projection (collective variable, CV) on the free energy surface (FES). Replica-exchange solute tempering (REST2) [50] falls into the first category, whereas metadynamics [51] belongs to the second category. We previously used REST2 simulations to investigate all-*anti* G-sequences capable of forming parallel G-hairpins and triplexes [34]. The work suggested that the perpendicular cross-hairpin orientation of G-tracts is more stable than the ideal Hoogsteen-paired G-hairpin and that the parallel G-triplex ensemble may be one of the possible transitory folding states but is not stable enough to represent a major long-lived intermediate.

In the present work, we used MD simulations to investigate transitory species involved in the folding of a parallel-stranded G4. We used a combination of the REST2 scheme [50] coupled with well-tempered metadynamics [51] (referred to as the ST-metaD method [52]) to accelerate the sampling. We simulated folding of a full G4 with $(GGGA)_3GGG$ sequence and characterized thermodynamic stabilities of

various G-hairpin and cross-hairpin ensembles, including ensembles formed by the GGGTTAGGG human telomeric sequence.

While our primary goal was to investigate the folding landscape of the complete parallel G4, as well as various G-hairpins, we also pursued two methodological goals. Firstly, we wanted to assess the sampling capability of the ST-metaD method to characterize folding of the full G4 and G-hairpins. It was shown recently that the ST-metaD method substantially outperforms the REST2 method alone and is very efficient for characterizing short RNA hairpin loops [53]. However, G4 and G-hairpins are much more challenging systems. Their free energy landscape is considerably more complex and G-hairpins are unstable species [34]. Secondly, we wanted to assess the performance of the force field to capture the folding free energy of G4s and intermediates.

Our simulations supported the view that folding of a full parallel three-quartet G4 $(GGGA)_3GGG$ starts with formation of a compacted coil-like ensemble of the G-strands. The G4 structure then emerges from this ensemble by multiple pathways without a single salient intermediate structure. The folding events proceed through a series of incremental conformational changes via cross-like structures, hairpins, slip-stranded and two-quartet G4 ensembles. The coil-like ensemble is likely to be coordinating at least one monovalent cation. The simulations also suggested that formation of guanine stacks in G-tracts (G-strands) is an important early phase of the folding process. The stacked G-tracts assemble into larger structures as semi-rigid blocks, which simplifies the search of conformational space by the DNA chain, resembling the diffusion collision model of protein folding [54,55]. The isolated G-hairpins are not stable, but they can be supported by additional interactions in the compacted coil-like ensemble. Besides obtaining insights into the G4 folding process, we also extensively assessed limitations of the force field, as the fully folded G4 was predicted to be thermodynamically unstable.

## 2. Materials and methods

### 2.1. Starting and reference structures

We performed all-atom explicit solvent MD simulations of DNA sequences GGGAGGGAGGGAGGG, GGGAGGGAGGG, GGGAGGG and GGGTTAGGG, starting from extended single-stranded chains. The starting structures were built using the Nucleic Acid Builder tool of AmberTools [56] as strands of a B-DNA helix with the complementary strand removed. The oligonucleotide structures are available in the Supplementary data. In each simulation, the molecules were biased to fold into a specific topology (G4, G-triplex or G-hairpin) defined by the reference structure (Fig. 2). Throughout the text, the *syn-anti* patterns of the G-tracts will be denoted by "*s*" (*syn*) and "*a*" (*anti*) in the designation of the topology, e.g., *aaa-aaa* means two all-*anti* G-tracts. The groove widths will be denoted by "w" for wide, "m" for medium and "n" for narrow. "H" in the sequence notation (e.g., $GGGH_nGGG$) denotes any nucleotide except G.

As a reference structure for folding the full G4, we used the first model of NMR structure PDB ID 2LEE [57]. For the triplex and GGGAGGG hairpin, residues G3 to G13 and G7 to G13 of 2LEE were used, respectively. As reference structures for the GGGTTAGGG hairpins, we used residues G2 to G10 from PDB ID 1KF1 [58] for the *aaa-aaa* hairpin and nucleotides G3 to G11, G9 to G17 and G15 to G23 from PDB ID 2GKU [59] for the *saa-saa*, *saa-ssa* wide-grooved and *ssa-saa* narrow-grooved hairpins, respectively. Reference structures for the *saa-ssa* narrow-grooved and *ssa-saa* wide-grooved hairpins were derived by manually flipping the middle base pair in the corresponding hairpin

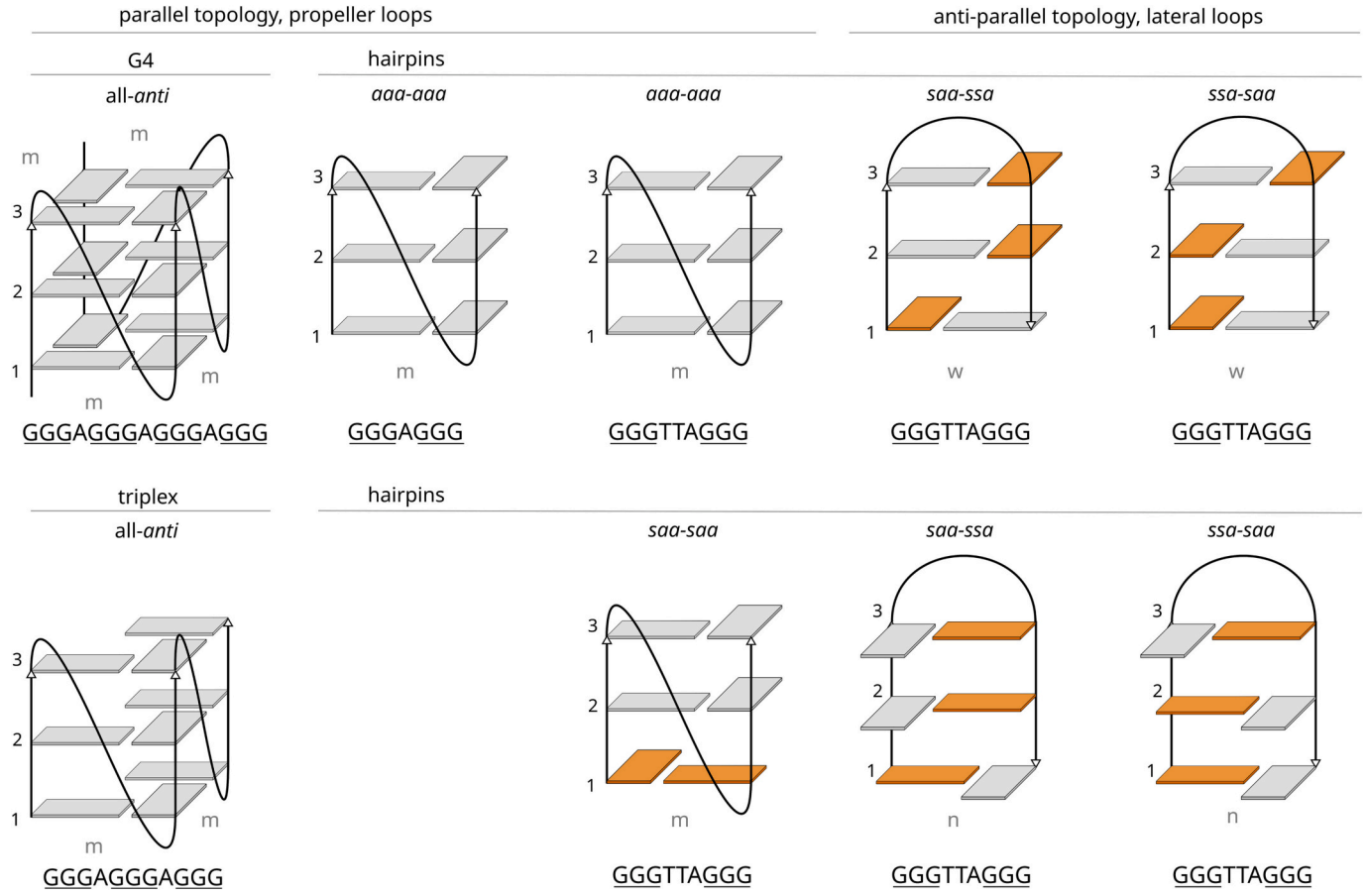


**Fig. 2.** Schematic representations of the reference structures. Bases in *anti* conformation are in gray, *syn* in orange. Letters above the hairpins denote the *syn*-anti patterns of G-tracts. Gray letters denote groove widths (wide, medium or narrow). Sequences of the simulated systems are shown below the reference structures.

taken from 2GKU, followed by proper equilibration of such a structure.

The DNA molecules were described by either the AMBER OL15 force field [60–65] or its upgraded OL21 version [66]. The molecules were solvated in octahedral boxes with the SPC/E [67] water model, and the simulations were performed under 0.15 M KCl salt (Joung & Cheatham parameters [68]). The GGGTTAGGG oligomer was also simulated under two other ionic conditions, namely net-neutralizing $K^+$ only and 1 M KCl. The minimal distance between the starting extended DNA strand and the water box border was set to 25 Å for the G4 and triplex and 15 Å for the hairpin sequences, respectively. For simulations with abasic loops, the charges on abasic nucleotides with hydrogen atoms attached to C1′ instead of N1/N9 were taken from ref. [69]. In three simulations, we supported guanine base-base H-bonds (N-H…N and N-H…O) with a HBfix potential [70,71], either by stabilizing only the "native" signature H-bonds or all possible guanine base-base H-bonds generally (gHBfix; only included guanine bases) [71].

### 2.2. Simulation protocol

The structures were first equilibrated by minimization with a gradual decrease of position restraints and heating. The SHAKE algorithm and hydrogen-mass-repartitioning [72] were employed to allow a 4 fs integration time step. Next, a 500 ns *nVT* simulation was run and starting structures for each replica were taken from equally distributed time intervals of that simulation. The initial velocities were randomized at the beginning of each simulation. The V-rescale thermostat [73] was used with a 0.1 ps coupling time constant to maintain the temperature at 298 K, whereas the pressure was not regulated to keep the volume constant.

In the ST-metaD scheme, the REST2 [50] protocol was used to run multiple simulations in parallel and allow individual trajectories to travel across replicas with different effective temperatures. Thus, in higher replicas, enthalpic barriers present in the solute were effectively downscaled. As a result, in higher replicas, the system could cross enthalpic barriers more easily, facilitating conformational sampling. In each replica, solute dihedral potentials and nonbonded interactions were scaled with a scaling factor $\lambda$ and solute–water interactions with $\sqrt{\lambda}$. $\lambda$ ranged from 1.00 to 0.60 for 12 replica runs and from 1.045 to 0.600 for 16 replica runs, resulting in an effective solute temperature of 500 K in the highest replica. The reference replica corresponded to $\lambda = 1.00$. One simulation was performed with a broader range of effective temperatures (266–700 K). Replica exchanges were attempted every 10 ps and acceptance rates ranged between 15 and 50 % and 20–60 % for the G4 and hairpins simulations, respectively. A lower acceptance was expected for systems with a larger solute.

The REST2 procedure aimed at accelerating the crossing of generic barriers. In the ST-metaD scheme, this acceleration was complemented with a more directed bias applied along a selected CV. This bias was built iteratively using metadynamics [51] independently on each replica. This meant that the bias potential specifically compensated for the free-energy difference present in each replica and made sampling of the CV more uniform. Specifically, the biased CV was based on εRMSD [74], which is a form of a contact matrix describing relative orientations of bases with respect to a reference structure. Thus, it provided a measure of the similarity of the base-contact (base pairing and stacking) pattern of the current structure compared to the reference structure. Different reference structures were used in the simulations, as detailed below, and were built using the proper fragments of PDB structures, as explained in Section 2.1. εRMSD was calculated only for guanines so that the loop conformation was not included in the CV. Augmented εRMSD with a cutoff of 3.2 was used for biasing, whereas standard εRMSD with a cutoff of 0.7 was used for analyses, as described in ref. [53]. This meant the biased εRMSD CV was less precise when determining the base-contact pattern but was more efficient for biased simulations, without compromising the precision of the analysis. In some simulations, an inter-tract εRMSD CV was used, where only the relative orientations of bases from different G-tracts were biased. In those cases, the mutual orientations of the bases within the same G-tract were not treated by the CV to eliminate the possibility that the CV artificially enhanced stacking within the G-tracts. The CV for *N* G-tracts was then defined as follows:

$$\varepsilon\mathrm{RMSD}_{inter-tract} = \sqrt{\frac{1}{3N}\left(3N \bullet \varepsilon\mathrm{RMSD}_{all}{}^2 - \sum_{i=1}^{N} 3 \bullet \varepsilon\mathrm{RMSD}_i{}^2\right)} \quad (1)$$

where $\varepsilon RMSD_{all}$ is calculated for all $3N$ guanines, and $\varepsilon RMSD_i$ is calculated only for guanines in the $i$-th G-tract. A schematic representation of the inter-tract εRMSD is provided in the Supplementary data, Fig. S1.

The Gromacs package (versions 2018 or 2021) [75] patched with PLUMED (versions 2.5.6 or 2.7.3) [76] was used to run the ST-MetaD simulations. All performed simulations are listed in Table 1. The parameter, coordinate and simulation settings files, reference structures, λ values and PLUMED input files are available in the Supplementary data. The calculated bias files, reference replica ensembles and selected demuxed trajectories (continuous trajectories traveling through the replica ladder) have been uploaded to the Zenodo database, DOI https://doi.org/10.5281/zenodo.8247280.

### 2.3. Analyses

The metadynamics bias typically converged on a timescale of a few μs, as shown by the $\Delta G_{fold}$ estimations in the Supplementary data (Figs. S2 and S3). Nevertheless, the $\Delta G_{fold}$ estimations fluctuated by ~1–2 kcal/mol over the course of the simulations. Hence, we used time averaging of the bias potential [77] over the second half of the trajectories. All reported $\Delta G_{fold}$ values are calculated from the time-averaged bias from the reference replicas. $\Delta G_{fold}$ values from independent simulations of the same system differed by about 1 kcal/mol. Thus, we estimated that the error in the data was around 1 kcal/mol and in the text, we report average $\Delta G_{fold}$ values from either two or three independent simulations with the same CV (regardless of the number of replicas), where applicable. Values from individual simulations are reported in the Supplementary data (Table S1). Further discussion on the statistical error in similar types of calculations can be found in ref. [53].

To determine whether the generated structures could be classified as folded, we used the εRMSD from the reference structure. A standard threshold of 0.7 for εRMSD was used to consider two structures as belonging to the same ensemble and to calculate $\Delta G_{fold}$. This threshold has been shown to be optimal for selecting structures with the same base contact pattern [78]. εRMSD was also used to identify different structural types (e.g., cross-hairpin or slip-stranded ensembles) in the G4 and hairpin simulations.

We also monitored the occurrence of hairpins and cross-hairpins in the simulation of the whole quadruplex. Thus, $\Delta G_{fold}$ values for hairpin and cross-hairpin ensembles formed by the $(GGGA)_3GGG$ sequence were derived from the G4-biasing simulation by selecting hairpin/cross-hairpin snapshots in the reference replica using εRMSD to the respective structures and subsequently calculating their weights based on the bias obtained from the G4 simulation. This enabled assessment of the impact of the context of the full quadruplex sequence on the stability of the G-hairpin and cross-hairpin structures. The protocol is detailed in the Supplementary data. $\Delta G_{fold}$ values of cross-hairpin and tilted ensembles in the hairpin-biasing simulations (i.e., simulations of the GGGAGGG and GGGTTAGGG sequences) were calculated in the same way.

While the reference replica was used for $\Delta G_{fold}$ calculations, we also monitored the development of continuous demuxed trajectories as they travelled through the replica ladder to visualize the folding events.

The G-tract stacking area was calculated as the sum of interaction surfaces between bases G1 and G2, and between G2 and G3. A cutoff of 80 $Å^2$ was used to consider the G-tract fully stacked. The cation

**Table 1**
Simulations reported in this study.

| Reference structure | Target loop topology, *syn-anti* G-tract pattern, groove width[a] | Force field | Number of replicas | Simulation length [μs][b] | Additional settings[c] |
|---|---|---|---|---|---|
| Sequence **GGGAGGGAGGGAGGG** | | | | | |
| Full G4 | Propeller, all-*anti*, m | OL21 | 16 | 3.7, 0.5 | Inter-tract CV |
| Hairpin[d] | Propeller, all-*anti*, m | OL21 | 16 | 2 | Inter-tract CV, only first two G-tracts biased |
| Full G4 | Propeller, all-*anti*, m | OL21 | 16 | 2 | Inter-tract CV, abasic loops |
| Full G4 | Propeller, all-*anti*, m | OL21 | 16 | 2 | Inter-tract CV, gHBfix (2 kcal/mol) |
| Sequence **GGGAGGGAGGG** | | | | | |
| Triplex | Propeller, all-*anti*, m | OL21 | 16 | 3 | |
| Sequence **GGGAGGG** | | | | | |
| Hairpin | Propeller, *aaa-aaa*, m | OL15 | 12 | 4.5 | |
| | | OL21 | 12 | 5 | |
| Sequence **GGGTTAGGG** | | | | | |
| Hairpin | Propeller, *aaa-aaa*, m | OL15 | 16 | 5, 5 | |
| | | OL15 | 12 | 5 | |
| | | OL15 | 16 | 5.5 | Inter-tract CV |
| | | OL15 | 12 | 5, 5 | Inter-tract CV, structure-specific HBfix (6 × 2 kcal/mol) |
| | | OL15 | 12 | 5, 5 | Inter-tract CV, gHBfix (2 kcal/mol) |
| | | OL15 | 12 | 4 | Net-neutralizing $K^+$ only |
| | | OL15 | 12 | 4 | 1 M KCl |
| | | OL15 | 12 | 4 | Abasic loop |
| | Propeller, *saa-saa*, m | OL15 | 16 | 5, 4 | |
| | Lateral, *saa-ssa*, w | OL15 | 16 | 4.5 | |
| | | OL15 | 12 | 5 | |
| | | OL15 | 16 | 5 | 266–700 K temperature range |
| | Lateral, *ssa-saa*, w | OL15 | 12 | 4.8 | |
| | Lateral, *saa-ssa*, n | OL15 | 12 | 4.8 | |
| | Lateral, *ssa-saa*, n | OL15 | 12 | 5 | |

[a] For structures, see Fig. 2.
[b] Two simulation lengths are reported when two independent simulations were run with identical settings.
[c] Unless stated otherwise, standard εRMSD was used as CV, an effective temperature range of 298–500 K was applied and no (g)HBfix was used.
[d] Although the full G4 sequence was simulated, only one G-hairpin (including the first two G-tracts) was used as a reference structure for the bias.

coordination number (*cn*) to evaluate $K^+$ binding in the G4 channel was calculated using distances between all cations and O6 atoms of guanines from two consecutive quartets (quartets *i* and *j*) as follows:

$$cn_{ij} = \sum_{k\in K^+}\sum_{l\in O6_{ij}}\left(1-\left(\frac{r_{kl}}{0.35}\right)^6\Big/1-\left(\frac{r_{kl}}{0.35}\right)^{18}\right) \quad (2)$$

where $r_{kl}$ is the instantaneous distance between a pair of $K^+$ and O6 atoms in nanometers.

## 3. Results

We performed enhanced-sampling folding simulations of a full parallel three-quartet G4 and several putative G4 folding intermediates, namely various G-hairpin topologies and a parallel G-triplex, to study their folding mechanisms and stabilities. The applied ST-metaD protocol with the εRMSD CV was able to capture hairpin and even complete G4 folding events. Each G4 folding event proceeded via a different route, but a shared feature was the initial formation of a coil ensemble. Our data further showed that stacked G-tracts are important elements in hairpin and G4 folding. For isolated $GGGH_nGGG$ sequences, the cross-hairpin ensemble was strongly preferred over the G-hairpin for the all-*anti* configuration due to interactions with the loop. The force field predicted that parallel hairpins with propeller loops were notably less stable than their antiparallel counterparts with lateral loops. The predicted $\Delta G_{fold}$ for a full parallel G4 was also positive, indicating force-field imbalances in the G4 description. In the following text, we first describe folding simulations of the full $(GGGA)_3GGG$ G4 and then simulations of GGGAGGG and GGGTTAGG hairpins.

### 3.1. Folding of the complete parallel G4 proceeds via a coil ensemble

We simulated the $(GGGA)_3GGG$ sequence biased to fold into a parallel G4 with single-nucleotide loops. In two simulations (3.7 and 0.5 μs long per replica) running with 16 replicas, we observed a total of six G4 folding events starting from the unfolded ensemble. Fig. 3 summarizes the formation of the individual structural elements of the G4 in the corresponding reactive trajectories; a reactive trajectory is part of the continuous trajectory which captures the transition from the unfolded state to the fully formed G4 structure state. We further observed one major subsequent refolding event involving partial G4 unfolding via strand-slippage of one G-tract and loosening of the outer quartets (Fig. 3a bottom, trajectory 6–2). The folding events are depicted in the Supplementary data, Videos S1–S6.

An important observation was that each of the folding events proceeded via a different path. However, the first step was typically the formation of a coil ensemble with at least one ion coordinated. The coil can be viewed as a broad ensemble of compacted structures stabilized by guanine base-base H-bond interactions (Fig. 4a) and was previously suggested as a possible intermediate in parallel G4 folding [19]. Afterwards, we mainly observed hairpin ensembles, slip-stranded ensembles and two-quartet G4s along the paths. Ideal cross-hairpin ensembles (as shown in Fig. 1e) were only formed in two folding trajectories, but the coil ensemble commonly featured cross-like states with only four, rather than six, guanines interacting. A variant of the cross-hairpin ensemble with fully stacked G-tracts is a tilted ensemble whose G-tract orientation is closer to the hairpin but not fully parallel. Again, the ideal tilted ensemble was seldom sampled, but tilted-like structures with four interacting guanines were more common. The three-layered G-triplex structure appeared in two folding events, immediately preceding formation of a full G4 in one of them. The other four folding events bypassed triplexes via different routes. In the last stage of folding, when two quartets were fully formed, the third layer typically consisted of two or three guanines. The remaining guanines were solvent-exposed and/or stacked with loop adenines. Once all the guanines were folded and the last quartet formed, a second cation was coordinated between the quartets as the last step. We also carried out standard unbiased simulations initiated from nearly-folded snapshots (data not shown), which revealed the same chronological order – first, the last quartet was formed and then a second cation was coordinated.

Since formation of the coil ensemble may have been induced by the CV used, we also performed one simulation with the sequence of the full

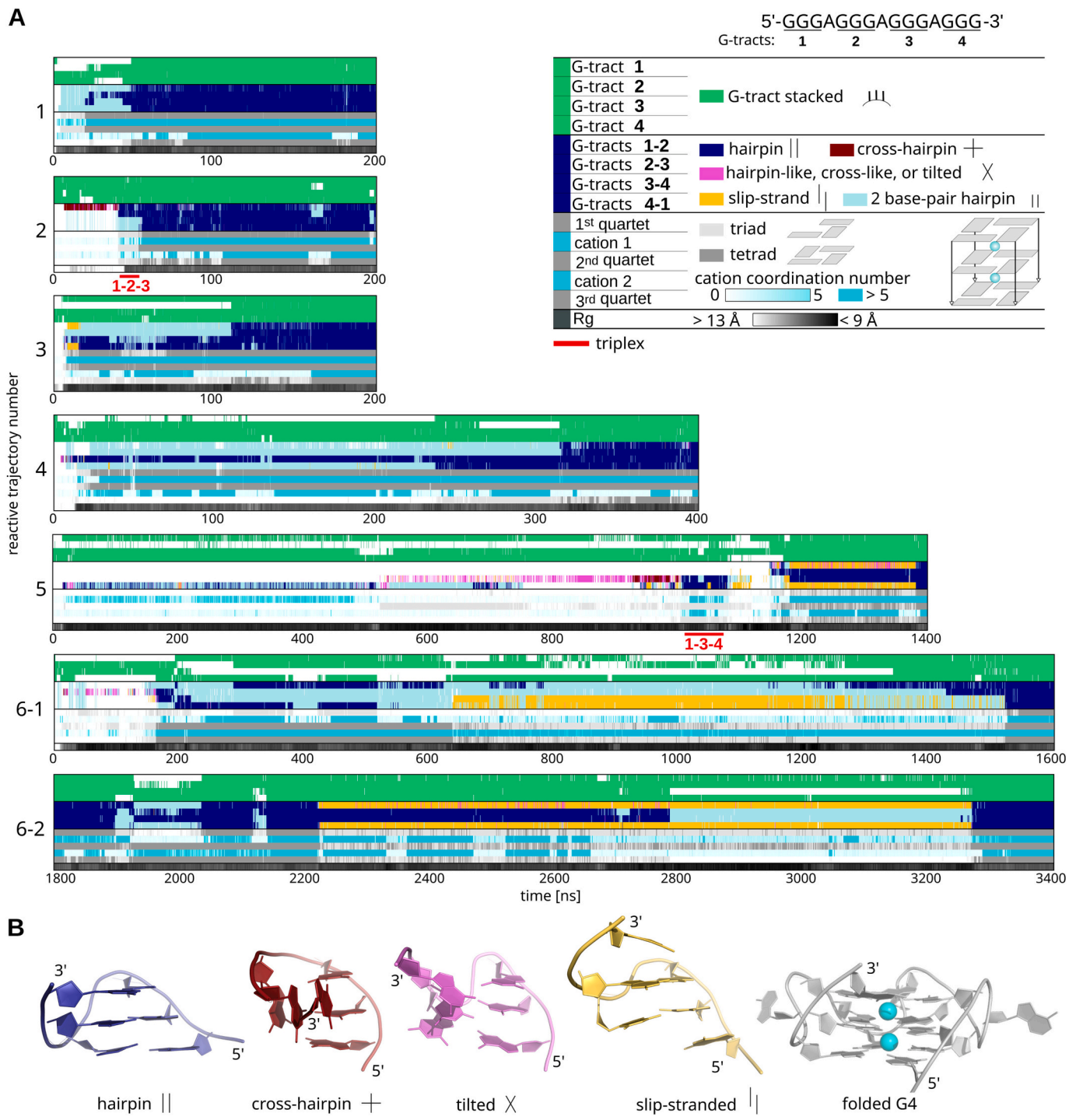


**Fig. 3.** Observed G4 folding events. (A) Time development of one refolding and six G4 folding events in six reactive trajectories. Individual lines in the graphs denote formation of selected key structural elements as shown in the legend. The first four lines monitor stacking in G-tracts. The next four lines monitor mutual orientations of two neighboring G-tracts; pink corresponds to a broader ensemble with $\varepsilon RMSD_{hairpin} < 1.0$, $\varepsilon RMSD_{cross} < 1.0$ and both G-tracts stacked, which encompasses the majority of tilted structures and hairpin/cross-hairpin structures with one nucleotide in *syn*. Cross-hairpin and tilted ensembles featuring only four guanines are not plotted. The next five lines monitor the formation of quartets and cation coordination between them, and the last line monitors the compaction of the structure by its radius of gyration (Rg). Once all the colors in the graph correspond to the colour panel on the left side of the legend, the G4 is fully folded. Red numbers below the triplex marks correspond to the indices of G-tracts forming the triplex. For reactive trajectory number 6, events are shown of initial folding (6–1) and subsequent refolding (6–2) in separate graphs. Timelines for full trajectories are shown in the Supplementary data (Figs. S4-S7). (B) Representative snapshots of some of the monitored structural elements formed by two G-tracts and the fully folded G4. (For interpretation of the references to colour in this figure legend, the reader is referred to the web version of this article.)

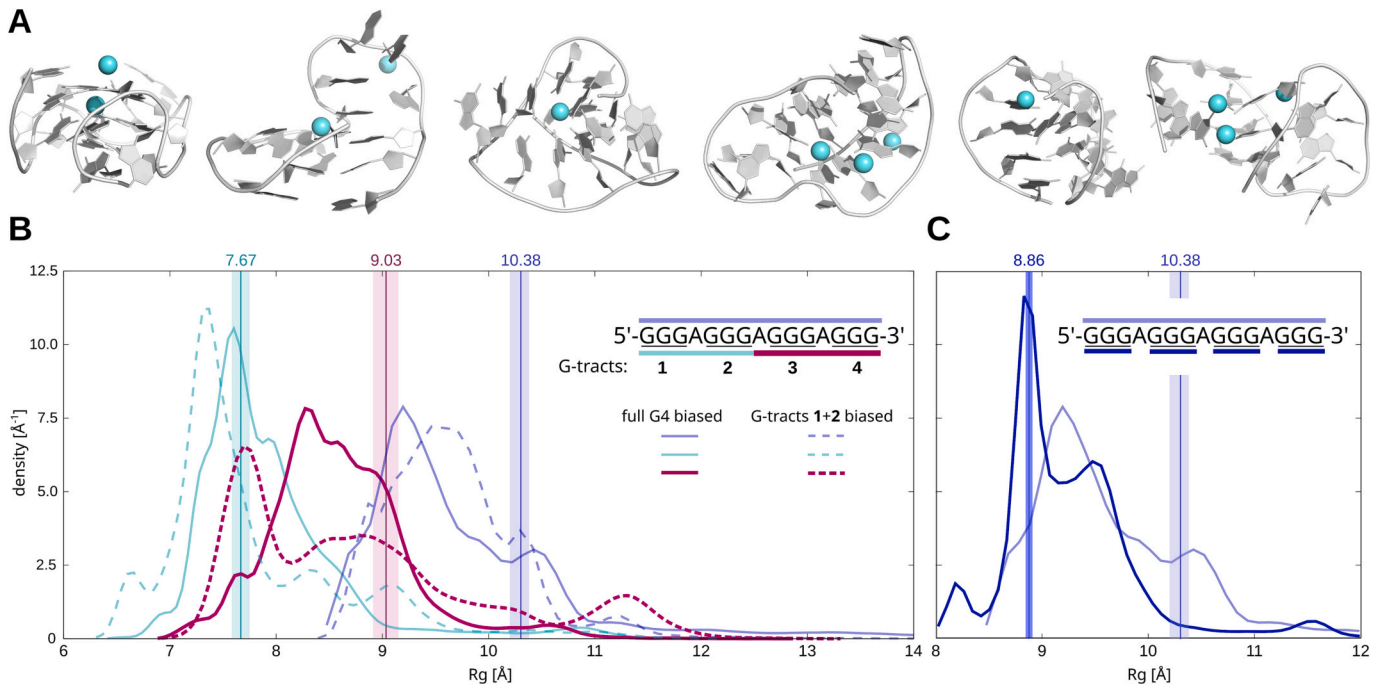


**Fig. 4.** Coil ensemble and radii of gyration in simulations of $(GGGA)_3GGG$ sequence. (A) Examples of coil-like structures. The first two structures are on-pathway G4 folding intermediates, the other four are off-pathway. All of them have Rg equal to or below the median value of the folded G4 (10.38). (B) Rg value distributions from reference replicas for the full G4 (violet) and its parts (GGGAGGG and AGGGAGGG, cyan and magenta, respectively) are shown with solid lines for simulations where all G-tracts were biased to fold and with dashed lines for the simulation where only the first two G-tracts were biased. The vertical lines show median values and interquartile ranges for the folded ensemble. Reweighted densities are shown in the Supplementary data (Fig. S8). (C) Comparison of histograms for G4 calculated with and without loop adenines. (For interpretation of the references to colour in this figure legend, the reader is referred to the web version of this article.)

G4 but with bias only on the first two G-tracts (to fold them into a hairpin, see Methods, Subsection 2.2). Although the biased folded hairpin could serve as a scaffold for the remaining two unbiased G-tracts, these never folded into a full G4 or at least triplex when the G-hairpin was formed. The simulation sampled a broader range of radii of gyration (Rg) values for the unbiased strand compared to the fully biased simulations, i.e., some more compact as well as some more extended states were sampled (Fig. 4b). This indicated that the coil ensemble was not induced by the CV.

The calculation of Rg also revealed that the exact value of overall compaction measured by the radius of gyration depended strongly on the inclusion/exclusion of loop residues (Fig. 4c). When only guanines were considered in the calculation of Rg, the distribution peak coincided well with the native state and the majority of other states had higher Rg (Fig. 4c). Nonetheless, structures within the limited range around the native Rg value did not only correspond to the native G4 and closely related structures but also included structures far away from the G4, as can be seen in the εRMSD distribution graph (Supplementary data, Fig. S9). When Rg of the whole molecule was calculated, most of the observed structures had Rg values smaller than the native G4 (Fig. 4b). These structures corresponded to the compacted coil ensemble (Fig. 4a). The results demonstrated that Rg is an ambiguous metric for assessing G4 folding, which has implications not only in computational studies but also in assessment of experimental data.

### 3.2. *Force field predicts a large positive value of the G4 folding free energy*

The ST-metaD simulation predicted a high positive $\Delta G_{fold}$ of +17 kcal/mol for the fully folded G4 (Table 2). Therefore, it was evident that the force field did not properly capture the balance between folded and unfolded ensembles. To the best of our knowledge, it is the largest free energy discrepancy in simulations of nucleic acids reported in the literature so far. Despite this, it was reasonable to assume that the simulations sampled relevant folding trajectories and the positive free energy of the native G4 structure did not invalidate the folding events reported above. The ST-metaD method was devised to sample high-energy states by flattening the FES, and thus found the native structure despite the high positive $\Delta G_{fold}$ value and evident large force-field imbalance over the overall FES. This force field issue will be discussed later in the paper. The parallel G-hairpin had a positive $\Delta G_{fold}$ of +18 kcal/mol, while the triplex was the least stable of the studied species with $\Delta G_{fold}$ of +20 kcal/mol (Table 2).

Demuxed (continuous) trajectories indicated that adenine stacking stabilized the unfolded states and slowed down the folding into the complete G4. A 2 μs simulation of the full G4 with abasic loops revealed a substantially lower $\Delta G_{fold}$ of about +9 kcal/mol. This simulation also sampled more (seven) folding events and showed principally the same mechanism as the $(GGGA)_3GGG$ simulations, proceeding through the

**Table 2**
Folding free energies for all-*anti* parallel G4, triplex, hairpin and cross-hairpin ensembles.

| Simulation | Simulated sequence | $\Delta G_{fold}$ [kcal/mol] | | | |
|---|---|---|---|---|---|
| | | G4 | Triplex | Hairpin[a] | Cross-hairpin[a] |
| G4 | $(GGGA)_3GGG$ | 16.9 | – | 14.4/8.3/11.1 | 12.1/5.5/8.6 |
| G4, only first two G-tracts biased | $(GGGA)_3GGG$ | – | – | 9.1/–/– | 6.0/–/– |
| Triplex | $(GGGA)_2GGG$ | | 20.1 | 8.2/6.1 | 5.7/3.0 |
| Hairpin | GGGAGGG | | | 17.8 | 6.8 |

[a] calculated as $\Delta G_{fold}$ considering only hairpins (cross-hairpins) 1-2/2-3/3-4, where the numbers denote the order of G-tracts in the strand (1-2-3-4), see Methods, Subsection 2.1 for details. "-" indicates that the structure was not sufficiently sampled.

coil ensemble via diverse pathways (Supplementary data, Fig. S10).

We attempted to stabilize the G4 by generally strengthening all pairs of possible guanine base-base H-bonds (i.e., by gHBfix, see Methods, Subsection 2.2). However, the extent of stabilization of the G4 fold was equivalent to the stabilization of the unfolded ensemble. Hence, the resulting $\Delta G_{fold}$ was (within the error margin) the same as without any force-field modification. Details are provided in the Supplementary data.

### 3.3. Parallel G-hairpins are stabilized inside the coil

Cross-hairpins were previously suggested to be more stable than parallel hairpins owing to their longer lifetimes in simulations [34]. We calculated the folding free energies of these structural elements from simulations of the full G4 sequence, triplex and isolated GGGAGGG sequence by selecting hairpin and cross-hairpin structure snapshots using εRMSD to these reference structures (see Methods, Subsection 2.2). While the simulations sampled similar structures (Supplementary data, Fig. S11), stabilities of the parallel hairpins calculated from the G4 and triplex simulations were notably higher ($\Delta G_{fold}$ less positive) than when only the isolated GGGAGGG sequence was simulated (Table 2). In other words, the parallel G-hairpins were stabilized inside the coil. The stability of the cross-hairpin ensemble was comparable in both cases.

### 3.4. Isolated parallel all-anti hairpins are less stable than antiparallel ones

We complemented the folding simulations of the full G4 and the isolated GGGAGGG hairpin with simulations of the isolated GGGTTAGGG sequence. In comparison to GGGAGGG, the GGGTTAGGG sequence can in principle form a broader spectrum of hairpin topologies, including antiparallel hairpins with lateral loops. While only six folding events were sampled within a cumulative time of 67.2 μs in simulations of the full $(GGGA)_3GGG$ G4, folding events were readily sampled in hairpin simulations (illustrated for the larger system with a TTA loop in Fig. 5). The folding free energies for the different topologies examined are provided in Table 3.

While the isolated ideally paired parallel all-*anti* GGGAGGG hairpin was extremely energetically unfavorable (+18 kcal/mol), the all-*anti* parallel hairpin formed by the GGGTTAGGG sequence had a lower, yet still high, $\Delta G_{fold}$ of about +12 kcal/mol (under all three ionic conditions tested; Fig. 6, Tables 3 and S1). The GGGTTAGGG parallel hairpin with one *syn-syn* pair was more stable than the all-*anti* one (Table 3 and Fig. 6). This may in part be due to the G7 intra-nucleotide N2-H2…OP H-bond, as suggested earlier [39]. Antiparallel hairpins with lateral loops formed by the GGGTTAGGG sequence were notably more stable than parallel hairpins with propeller loops in our simulations (Table 3 and Fig. 6). Data for two distinct target parallel and four antiparallel hairpins clearly confirmed this trend.

**Table 3**
Folding free energies of the studied isolated hairpins.

| hairpin topology | $\Delta G_{fold}$ [kcal/mol] |
|---|---|
| Sequence **GGGAGGG** | |
| Parallel, *aaa-aaa*, m | 17.8 |
| Sequence **GGGTTAGGG** | |
| Parallel, *aaa-aaa*, m | 11.8 |
| Parallel, *saa-saa*, m | 8.2 |
| Antiparallel, *saa-ssa*, w | 5.9 |
| Antiparallel, *ssa-saa*, w | 5.1 |
| Antiparallel, *saa-ssa*, n | 4.2 |
| Antiparallel, *ssa-saa*, n | 5.7 |

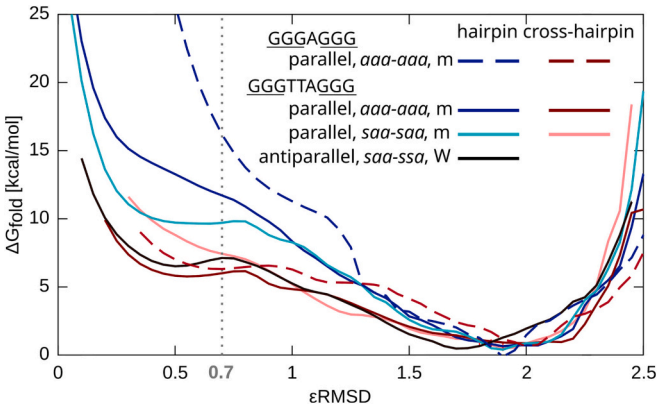


**Fig. 6.** $\Delta G_{fold}$ along the εRMSD CV for GGGAGGG and GGGTTAGGG sequences folding to different reference structures. $\Delta G_{fold}$ for cross-hairpin ensembles were calculated from the respective hairpin-biased simulations. Time-averaged bias potentials from the reference replica only were used to calculate $\Delta G_{fold}$. The bin width used to generate the plot was 0.01.

In the case of the GGGTTAGGG *aaa-aaa* parallel hairpin, we also considered an ensemble with all guanines in the *anti* conformation to estimate $\Delta G_{fold}$ (by removing all other snapshots from the reference replica). This effectively eliminated competition with other possible GGGTTAGGG hairpin folds and their on-pathway states. The hairpin stability then increased by ~3 kcal/mol, which was still above values for antiparallel hairpins (antiparallel hairpins are stabilized by ~1–3 kcal/mol when considering only their target *syn-anti* pattern in the ensemble). We also tried to stabilize the *aaa-aaa* hairpin by supporting formation of each of the six structure-specific guanine-guanine H-bonds with a 2 kcal/mol HBfix potential. Such a dramatic intervention, i.e.,

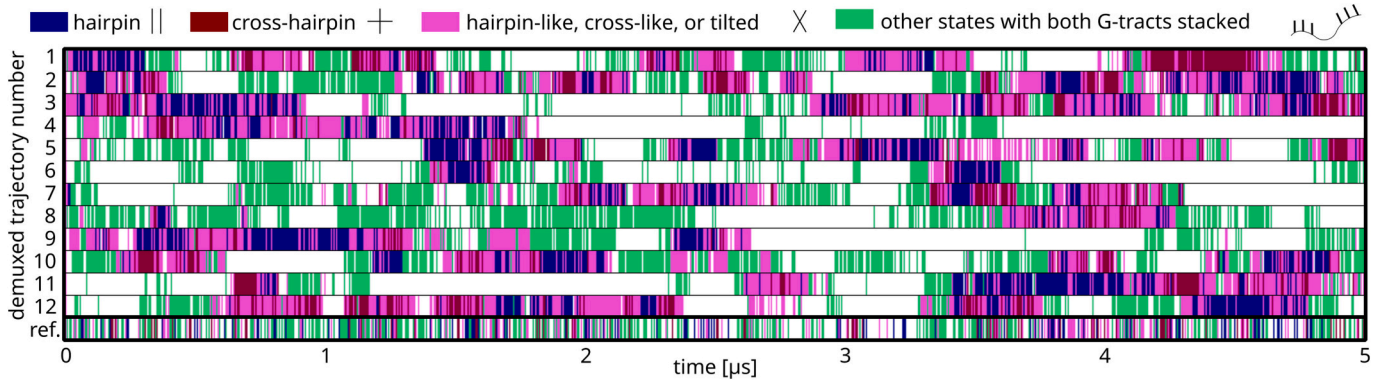


**Fig. 5.** Development in twelve individual demuxed (continuous) trajectories in one GGGTTAGGG *aaa-aaa* folding simulation. The reference replica is plotted at the bottom. For details of the colour-coded ensembles, see the caption of Fig. 3; green colour in this figure corresponds to all other states with each G-tract having stacked guanines. (For interpretation of the references to colour in this figure legend, the reader is referred to the web version of this article.)

stabilization of the hairpin state by 12.0 kcal/mol, resulted in a $\Delta G_{fold}$ value of about 2.7 kcal/mol while also stabilizing some structures in the unfolded ensemble. However, stabilizing the hairpin fold did not result in increased sampling of the folding events (Supplementary data, Fig. S12). gHBfix had a smaller but opposite effect, stabilizing the unfolded ensemble ($\Delta G_{fold}$ of the hairpin +14 kcal/mol).

### 3.5. Cross-hairpin ensembles are stabilized by interactions with the loop

Cross-hairpin ensembles were more stable than hairpins for the isolated $GGGH_nGGG$ sequences (Fig. 6). $\Delta G_{fold}$ values for the all-*anti* cross-hairpin ensembles of the GGGAGGG and GGGTTAGGG sequences were +6 and +5 kcal/mol, respectively. $\Delta G_{fold}$ for the tilted ensembles was about +9 kcal/mol in both cases. The cross-hairpin ensemble of the GGGTTAGGG sequence was stabilized by diverse additional stacking and H-bonding interactions with the loop residues (an example is shown in Fig. 7a). Antiparallel hairpins were stabilized by lateral loops in a similar fashion. The GGGAGGG sequence formed lesser interactions between the G-tracts and loop. Loop residue A4 was able to stack on either G3 or G5, but no H-bonds between the loop and guanines were formed in the GGGAGGG cross-hairpin ensemble.

Solvent-exposed bases of propeller loops were expected to introduce an entropic penalty for parallel hairpins compared to loops stabilizing the folded antiparallel hairpins or cross-hairpins. Indeed, simulations with an abasic loop predicted $\Delta G_{fold}$ of about +10 and +7 kcal/mol for the GGGTTAGGG *aaa-aaa* hairpin and cross-hairpin ensembles, respectively.

In the GGGTTAGGG sequence with *saa-saa* configuration, formation of the full cross-hairpin or tilted structures with all six guanines H-bonded (as shown in Fig. 3b for the all-*anti* configuration) was not observed. In contrast to the all-*anti* configuration, the *syn*-configuration of the bases did not allow the creation of compatible H-bond donor-acceptor patterns along the whole G-tract. When cross-hairpin or tilted structures were sampled, they had the *anti*-bases H-bonded, but one or no *syn*-base was involved in the inter-tract binding (Fig. 7b). Thus, only five or four bases participated in the cross, similar to the cross-like ensembles involving four bases seen in the full G4 folding simulations. The $\Delta G_{fold}$ for the *saa-saa* cross-hairpin ensemble was about 1.5 kcal/mol lower than that of the hairpin. Thus, the difference was not as pronounced as for the *aaa-aaa* configurations (Fig. 6). Finally, cross-hairpin ensembles featuring a G-tract with two *syn* nucleotides were not observed.

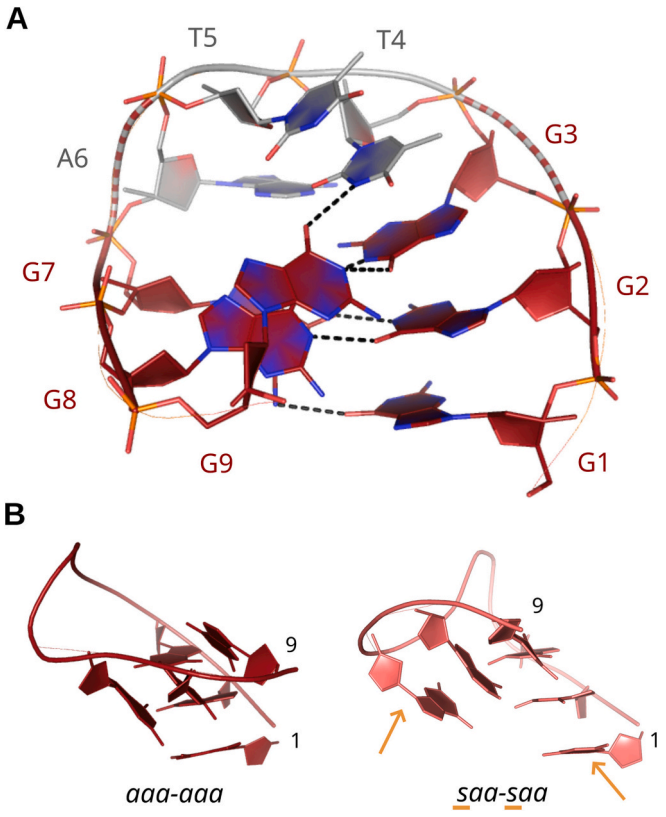


**Fig. 7.** Cross-hairpin structures. (A) Example of loop interactions stabilizing the GGGTTAGGG cross-hairpin structure. H-bonds are marked with dashes. T4 stacks with G3 and H-bonds to G9. A6 can also stack with G7 to stabilize the cross-hairpin. (B) Comparison of *aaa-aaa* and *saa-saa* cross-hairpins. H-bonding with T4 was also observed in the *saa-saa* cross ensemble (not shown). Bases in *syn* are indicated by orange arrows.

### 3.6. Hairpin formation proceeds mainly by stacked G-tracts orienting themselves with respect to each other in the space

In the demuxed folding trajectories of all the systems, we commonly observed formation of G-tract stacks, i.e., stacking of three consecutive guanines. These stacked G-tracts then searched the space to eventually form the target hairpin (Fig. 5). The chosen CV may have driven the formation of the G-stacking in G-tracts in our hairpin-folding simulations as we targeted the relative orientations of guanine bases (described with εRMSD, see Methods, Subsection 2.2). Thus, we performed one additional hairpin simulation with a modified inter-tract εRMSD CV that did not affect mutual orientations of guanines within G-tracts. However, G-tract stacking was only slightly less sampled so that stacked G-tracts were still clearly formed (Supplementary data, Fig. S13). Analysis of our previously published REST2 trajectories [34] revealed about 75 % of the population of each individual G-tract was fully stacked for the GGGAGGG simulation, and the number was 40 % for the GGGTTAGGG sequence (Supplementary data, Table S2). Thus, formation of stacking within the G-tracts seems relevant to actual folding mechanisms. However, base stacking has been suggested to be overestimated by the AMBER force field [79–81]. Therefore, the magnitude of GGG stacking in our simulations may have been overestimated by the force field.

### 3.7. Sampling problem on the rich FES

In general, multiple folding events were observed in hairpin simulations, although some demuxed trajectories did not sample hairpin folding events at all (Supplementary data, Table S1 and Fig. S12). This indicates that the simulations were not fully converged, as full convergence would imply that all demuxed trajectories sampled similar populations of different structures. Convergence of the sampling in individual trajectories was even poorer in G4 simulations. This is not surprising given the rich structural dynamics of the studied systems and their high free-energy instability. The individual demuxed trajectories sufficiently sampled all replicas in the ladder (Supplementary data, Fig. S14). However, other than the target (biased) hairpin topology was rarely sampled in the simulations, despite no restraints on glycosidic or backbone torsions being applied. For example, the parallel GGGTTAGGG *saa-saa* hairpin was sampled in 0.06 % of snapshots in simulations targeting the *aaa-aaa* hairpin but not at all in simulations targeting the lateral loops. The very unstable *aaa-aaa* hairpin was not sampled in the *saa-saa* simulation, whereas the *aaa-aaa* cross-hairpin was. For the more stable antiparallel hairpins, both wide and narrow groove topologies with the same *syn-anti* patterns were readily sampled in simulations, despite only one of them being targeted in a particular simulation. Sampling of both types of hairpins with the same *syn-anti* pattern in one simulation may have been supported by the CV biasing the G-tracts to the same respective glycosidic patterns. The wide and narrow groove topologies with the same glycosidic patterns differed in εRMSD by ~1.4.

This sampling issue was also demonstrated by limited overlap of the unfolded ensembles of simulations targeting different hairpin topologies

(see Supplementary data for details). On the other hand, changes in the simulation protocol (number of replicas, different scaling factors) did not affect the results (Supplementary data, Table S1 and Fig. S11). This indicates that the methodology was reasonably robust but at the limits of what can be achieved with contemporary methods and computers.

## 4. Discussion

We carried out a series of ST-metaD enhanced-sampling folding simulations targeting a three-quartet parallel-stranded DNA quadruplex $(GGGA)_3GGG$ and several isolated G-hairpin topologies. The goal was to better understand G4 folding, the roles of selected intermediates and, mainly, to visualize transient structures. We wanted to predict the types of structures that could occur along the folding pathways and expected that the ST-metaD method would be sufficiently robust for this purpose. However, it became obvious that capturing complete G4 folding using unbiased MD simulations is presently beyond the capabilities of contemporary computers, as well as force fields.

The folding simulation of the $(GGGA)_3GGG$ G4 predicted $\Delta G_{fold}$ of +17 kcal/mol. This was in clear disagreement with experiments and showed the magnitude of the overall imbalance in the force field (see below, Subsection 4.2). Nevertheless, our simulations still provided useful insights into the folding mechanism of the all-*anti* parallel-stranded G4. The metadynamics method flattened the free energy landscape along the chosen CV, and thus allowed folding events to be sampled even in cases where the target structure had a positive free energy. The simulations showed that folding of the parallel-stranded G4 was a multi-pathway process involving the structuring of quartets inside a compact coil ensemble.

When considering ideal Hoogsteen-paired structures, the isolated parallel all-*anti* G-hairpins were predicted to be strikingly unstable with $\Delta G_{fold}$ of +18 and +12 kcal/mol for the GGGAGGG and GGGTTAGGG sequences, respectively (Table 3). As discussed below, these high instabilities may partly reflect inaccuracies of the simulation force field. Formation of cross-hairpin ensembles that are on pathway ensembles to the parallel G-hairpin was a more likely event for isolated sequences. Antiparallel GGGTTAGGG G-hairpins were predicted to be more stable with $\Delta G_{fold}$ ranging from +4 to +6 kcal/mol. The simulations revealed very rich unfolded ensembles for the studied sequences, with a plethora of competing states, and did not indicate the existence of a single stable structure for the hairpin sequences.

### 4.1. Suggested properties of the parallel G4 folding landscape

Despite the evident force field and sampling limitations, we suggest that the observed folding events (Fig. 3) provide useful insights into the nature of folding pathways and transitory ensembles sampled during folding. Our simulations revealed that the conformational landscape of G4 sequences is extremely rich.

The suggested folding process of a parallel G4 (assuming an entirely unstructured starting ensemble) based on the simulations is summarized in Fig. 8. First, extended G-tract chains form stacked G-tracts with occasional fraying of one of the three stacked guanines. These tracts then explore the conformational space and position themselves with respect to each other in many possible ways. They tend to assemble into larger structures as semi-rigid blocks. This simplifies the search of conformational space by the DNA chain, resembling the diffusion collision model of protein folding with prefolded α-helices. The parallel G4 folding proceeds from extended chains via formation of a coil ensemble (Fig. 4a). The coil can be viewed as a broad ensemble of compacted structures stabilized by guanine base-base H-bond interactions. Coil ensembles coordinating at least one cation have been previously suggested as folding intermediates for parallel G4s in computational and experimental studies [14,22,25,34,82]. The compacted coil ensemble can be likened to the molten globule state in protein folding. Despite all collapsing initially into the coil ensemble, each of the six simulated G4 folding events proceeds via a different path (Fig. 3a). Thus, the observed folding events do not represent a simple pathway via some salient intermediates. Instead, the final G4 structure emerges from the compacted unfolded ensemble via numerous incremental conformational changes. Native interactions are formed from inside the coil and the ensemble diffuses via different possible orientations of the G-tracts, cross-like, hairpin and slip-stranded structures until a G4 is formed. Our results suggest that the G-triplex is not a mandatory intermediate on the parallel G4 folding landscape and can be easily bypassed. Occasional events of coil untying and partial chain extension allow major structural

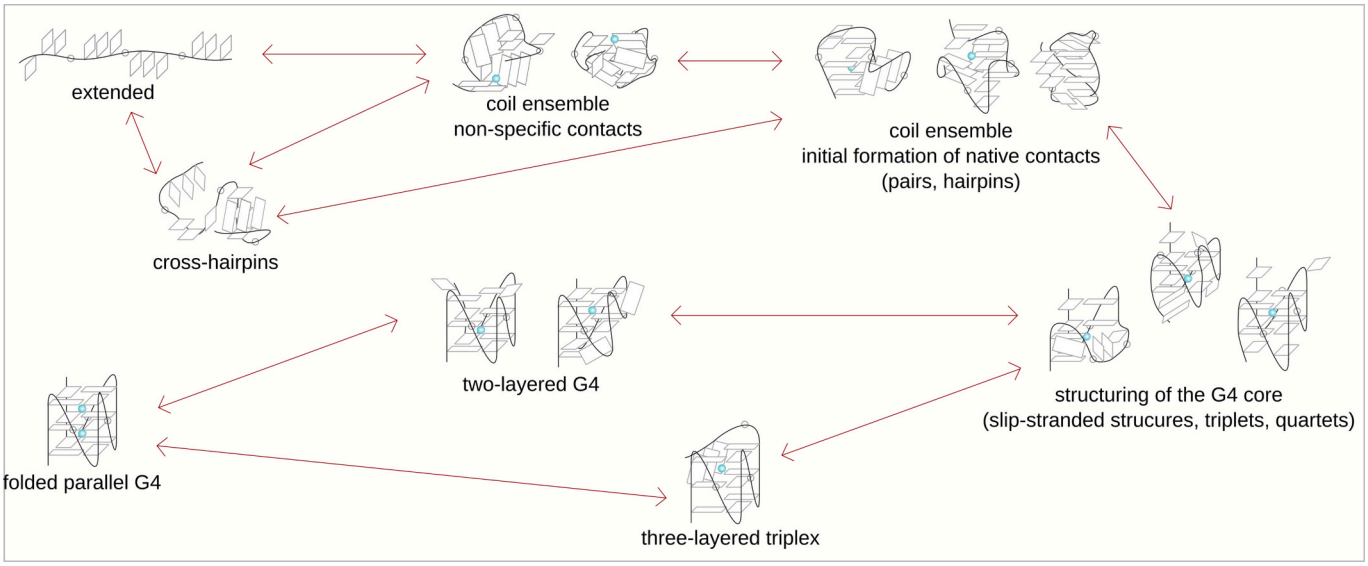


**Fig. 8.** Summary of the single-nucleotide-loop parallel G4 folding process based on the presented simulations. Folding is initiated by the formation of a compact coil structure, within which the native interactions form gradually. Loop nucleotides are represented by circles on the backbone. They can also participate in stacking interactions with the guanines. The structures shown are representatives of the broader ensembles they are parts of. Antiparallel species are not included in the scheme, although they are likely to be present in the early-stage coil ensemble. Note that although we suggest that ST-metaD simulations may reliably identify types of transitory structures that participate in the folding, they do not provide any kinetic information. The depicted intermediates are not necessarily stable species and may belong to the transition ensembles.

rearrangements. Indeed, such chain extension events were sampled in the partially biased G4 simulation, as illustrated by the range of compactness in Fig. 4b. The $(GGGA)_3GGG$ sequence can, in theory, also form an antiparallel Hoogsteen-paired hairpin featuring only two G-pairs and a two-nucleotide lateral loop. Such species did not occur in our simulations, likely due to the limited sampling, but we expect them to be present on the parallel G4 folding landscape, which may be consistent with some experimental observations [22,82].

A similar folding mechanism may apply for a parallel-stranded RNA G4. The compacted coil-like ensemble we predicted here for the full DNA G4 may be related to the hydrophobic collapse suggested by experiments for the initial phase of folding of RNA G4s [83]. There are also similarities with the multi-pathway gradual emergence of RNA G4 from cross-like intermediates indirectly suggested by MD simulations [33].

Loop conformational degrees of freedom add another layer of complexity to the folding process. Simulations with abasic loops showed notably lower $\Delta G_{fold}$ for the G4 and a decrease of the $\Delta G_{fold}$ difference between the *aaa-aaa* hairpin and cross-hairpin, confirming the effect of the loop residues on their stabilities. Consistently, stabilization of the G4 fold upon removal of loop bases has been reported for a single-nucleotide G4 in melting experiments [11]. This may be due to the elimination of adenine-stabilized unfolded structures as well as reduction of the entropic penalty introduced by the otherwise solvent-exposed adenine base in the folded G4 [11,84].

A single isolated hairpin sequence has the properties of a disordered chain and transits among a plethora of competing states. Spontaneous formation of a parallel hairpin without external stabilizing interactions was notably less likely than formation of antiparallel hairpins and cross-hairpins, which are stabilized by the loop residues (Fig. 6, Table 3). Cross-hairpin ensembles can be formed by *aaa-aaa* and, to some extent, *saa-saa syn-anti* patterns. The cross-hairpin ensemble can lead to a parallel hairpin by rotating the relative orientations of the two G-tracts. The relative difference in the stabilities of the parallel hairpin and cross-hairpin decreases when the sequence is embedded in a longer context (Table 2). Residues preceding and following the GGGAGGG motif and interactions inside the G4 coil ensemble can stabilize the parallel hairpin, consistent with our previous simulations of a G-triplex showing that it could be stabilized by flanking nucleotides or stacking with hemin ligand [34]. When part of a complete G4-forming sequence, the cross-hairpin and hairpin ensembles can form from an extended, unfolded single strand independently of the other G-tracts, or they can be generated gradually inside the coil-like structure (Fig. 3). Indeed, the isolated hairpin does not behave exactly as it would if it were embedded in the complete G4 sequence. The folding intermediates and pathways observed in the simulations of isolated hairpin sequences qualitatively corresponded to hairpin-folding pathways observed in the simulation of the full G4 sequence, although the cross-hairpin ensemble was a less frequent on-pathway intermediate in the latter (Supplementary data, Fig. S11). This was expected as the full G4 sequence can in principle follow pathways in addition to those including hairpin-like structures. In summary, cross-hairpin structures may be more relevant than G-hairpins during the initial phases of folding when the DNA strand is relatively extended and individual G-tracts approach each other (initial phases of nucleation of the coil). The hairpins may be later structured inside the coil. While the cross-hairpin ensemble is suggested to dominate over the hairpin for the all-*anti* configuration in an extended (uncompacted) chain, the difference is not as pronounced for the *saa-saa* configuration. The lower likelihood of transition to the cross-hairpin might be one of the reasons for the higher stability of the *saa-saa* compared to *aaa-aaa* configuration.

Given the apparently different properties of putative on-pathway folding intermediates for different G4 topologies (e.g., parallel and antiparallel hairpins studied here), the suggested folding mechanism cannot be simply generalized outside the context of the studied $(GGGA)_3GGG$ G4. In fact, even similar G4s can follow distinct folding mechanisms [82]. Our data showed that parallel hairpins need to be stabilized inside the coil, but antiparallel ones can probably form more easily and at earlier stages of folding events. Although the initiation of folding of a parallel G4 with one parallel hairpin formed and the rest of the chain extended is unlikely, such a scenario may be possible for G4s containing antiparallel hairpins. Yang et al. previously reported such a folding pathway for a two-quartet antiparallel G4 of the thrombin-binding aptamer (15-TBA) with lateral loops [32]. Their simulation data suggested that folding proceeded first through a hairpin-like base-collapsed ensemble, where one native lateral loop was already formed and the rest of the bases were paired non-specifically, and then the chain eventually structured into a triplex. The last step was binding the last GG tract, either directly or via a strand slip. Bian et al. combined all-atom simulations with a structure-based coarse-grain model to study folding of the human telomeric G4 sequence into two different hybrid topologies [49]. The first folding step predicted was formation of an antiparallel hairpin connecting the 5′ and 3′-end G-tracts. The two topologies studied by Bian et al. folded via separate pathways with different complexities, and only one of them transited via a triplex ensemble.

Finally, we observed that the (in)stability of the parallel hairpin GGGTTAGGG did not depend on the cation concentration (Supplementary data, Table S1). This may seem counterintuitive since the dominant G4 topology (parallel, 3 + 1 hybrids, 2 + 2 antiparallel) formed by the human telomeric sequence (as well as various other sequences with several nucleotides in the loops) depends on the cation nature and concentration [85,86]. However, the isolated hairpin is only a weak cation binder, explaining our results. This observation is also consistent with our previous hypothesis that the dependence of the dominant topology on cation conditions is significantly driven by the (in)stability of late-stage slip-stranded parallel G4s, not the hairpin [13]. One should bear in mind that due to the CV used (see Section 4.3 below for further discussion), our calculations only focused on a dissected part of the free-energy landscape pertinent to the parallel G4 and did not explore (re) folding into other possible G4 topologies. In addition, we monitored the folding with respect to an initial unstructured state and did not consider formation of prefolded structures, which may occur in experiments.

### 4.2. Force field struggles to accurately capture the global G4 folding landscape

Although the present simulations provided unique insights into the G4 folding landscape, they were obviously limited by the force-field accuracy, selected CV and achievable sampling. The most striking indicator of force field issues was the positive value of $\Delta G_{fold}$ of +17 kcal/mol calculated for the $(GGGA)_3GGG$ G4. In comparison, $\Delta G_{fold}$ for the $(GGGA)_3GGG$ G4 estimated from melting curves in 1 mM KCl solution was about −1.4 kcal/mol [11]. The exact value depends on the experimental setup, but the studied G4 should have a negative $\Delta G_{fold}$. Since our simulated unfolded ensembles did not cover the whole real space of unfolded ensembles, the predicted positive $\Delta G_{fold}$ may still have been underestimated. This may be surprising since standard simulations of folded cation-stabilized quadruplexes are very stable. Hence, quadruplexes have usually been assumed to be well-described by the force field [19]. Apparently, this is not true for their global free energy landscape.

A positive folding value (albeit much smaller) with the AMBER force field has been reported earlier by Yang et al. for 15-TBA [32]. Yang et al. suggested that H-bonding in quartets is understabilized by the AMBER force field non-bonded terms. They proposed a correction based on modification of the van der Waals parameters using the non-bonded fix (NBfix) approach, which increased the stability of 15-TBA by ~6.5 kcal/mol (from +3.8 kcal/mol to −2.8 kcal/mol), i.e., by ~3 kcal/mol per quartet. In our study, use of a general (not structure-specific) force field correction to increase the guanine base-base H-bond strength (gHBfix) did not improve the $(GGGA)_3GGG$ G4 stability. The balance of H-bond strengths in quartets and the unfolded ensemble may explain the positive folding energy, but the understabilization of $(GGGA)_3GGG$ was

evidently much larger than that of 15-TBA.

Another known force-field issue is the overestimation of ion-ion repulsion in the G4 channel due to missing polarization/charge transfer effects with fixed point charges force fields [87]. Our folding trajectories suggested that binding of the second ion was the last step in the folding process after all the quartets were fully assembled. Nevertheless, it is possible that binding of the second ion proceeds faster and at an earlier stage of the folding. It is likely that over-estimation of ion-ion repulsion (which does not affect simulations of the two-quartet 15-TBA with just one internal cation) contributed to the unsatisfactory $\Delta G_{fold}$ of the three-quartet quadruplex. The magnitude of this effect is presently not clear. However, overestimation of inter-cation repulsion may in future be resolved by using polarizable force fields [88,89].

Further, it is possible that the force field understabilized propeller loops, as has been tentatively suggested in the past. Previous unbiased and temperature-accelerated MD studies reported fast unfolding (short lifetimes) for all-*anti* hairpins, triplexes and G4s (the latter simulated in the absence of cations) with propeller loops. Longer lifetimes were observed for structures with propeller loops with at least one guanosine in *syn* and structures with lateral and diagonal loops [28,34,36,39,90]. This is consistent with the extraordinary instability of the parallel all-*anti* hairpin with the propeller loop seen in the present study, which was for the first time quantified by calculation of $\Delta G_{fold}$ (Table 3). However, it is unclear which parts of the force field are responsible for the imbalanced description of propeller loops. It does not appear to be caused by dihedral parametrizations, as differences in dihedral parameters of recent refinements of the AMBER force field are too subtle. For example, the α/γ dihedral correction introduced in the OL21 DNA force-field update of the OL15 version improved B-DNA and *Z*-DNA descriptions [66,91] but did not improve the stability of the G-hairpins simulated here (Supplementary data, Table S3).

### 4.3. Exploration of the FES is limited for such complex systems

Despite the predicted positive free energy of all target species, we were still able to characterize the folding events using the metadynamics part of the simulation protocol, as the metadynamics flattens the FES along the selected CV. The ST-metaD approach combined well-tempered metadynamics with εRMSD CV biasing the simulations toward the target structures with a REST2 replica-exchange protocol to accelerate sampling of the remaining degrees of freedom. Due to the richness of the studied systems' FES, fully converged conformational ensembles are still out of our reach even for G-hairpins simulated with enhanced-sampling protocols. Isolated G-hairpins are inherently unstable species, which further complicates their study with unbiased MD simulations. The chosen CVs (i.e., direction in which the bias is applied to guide the conformational sampling) may also affect the sampled states and folding pathways [92]. The ST-metaD protocol applied here could capture the formation of very unstable (in the force-field description) species, including folding of a full three-quartet G4, and enable prediction of their $\Delta G_{fold}$. However, the present simulations remain far from quantitative convergence and exploration of the unfolded conformational space is affected (restricted) by the specific CV chosen (Supplementary data, Fig. S15). Nevertheless, we believe that the ST-metaD method is robust enough to qualitatively study molecules with a complex FES and elusive processes such as G4 folding, although the latter is probably only possible in the vicinity of one specific fold (folding funnel) to which the CV is linked. We note that a similar technique of parallel tempering combined with metadynamics using 2D bias defined by εRMSD and RMSD was successfully used in the above-mentioned simulations of the 15-TBA G4 [32,37].

Our results suggested that the employed CV affected the folding pathways of the full G4 more than those of isolated hairpins. At the same time, G4 folding landscapes are very complex and cannot be fully captured by a single simple CV. Nevertheless, the $(GGGA)_3GGG$ sequence only forms one dominant G4 topology – the parallel one. Thus, the effect of the CV choice on the free-energy landscape is likely to be less significant than it would be, for example, for the highly polymorphic human telomeric sequence. A comparative partly biased simulation with only the first two G-tracts biased by the CV revealed that the coil ensemble was also readily sampled in the unbiased segment, although its properties slightly differed, i.e., it tended to be more compacted than in the fully biased simulation (Fig. 4b). Thus, both biased and partly biased simulations supported the existence of the coil ensemble. The differences may not invalidate the observed folding events, but rather suggest other alternative pathways that are poorly captured by the employed CV, which nevertheless still likely proceed through the coil ensemble.

To assess the choice of CV, Rg is commonly monitored in G4 simulations, and sometimes even in experiments [93], as it is assumed to measure how well a given molecule is folded. The presumption is that high Rg corresponds to unfolded states and the lowest Rg to the compact fully-folded G4 structure. However, the distribution of Rg observed in our folding simulations revealed that the coiled ensemble had a lower Rg than the native G4 (Fig. 4 and Supplementary data, Fig. S8), as we have suggested before in simulations of misfolded structures [94]. Thus, Rg is not a sufficient metric for discriminating between folded and unfolded states. In simulations, this issue could be alleviated by considering Rg of just the G4 core (without the loops), possibly combined with another CV, but in experimental Rg measurements, it is not possible to selectively exclude parts of the molecule.

## 5. Conclusions

Characterization of G4 folding pathways, including transitory ensembles, can help to elucidate G4 properties and roles. However, because characterization of short-lived intermediates and transitory ensembles cannot be achieved by experimentation, computational modeling and simulation studies are required [19,20]. Here, we report a series of all-atom enhanced-sampling folding simulations that demonstrated formation of the complete parallel three-quartet DNA $(GGGA)_3GGG$ G4 from an extended unfolded strand.

ST-metaD simulations suggested that folding of the parallel G4 proceeded by multi-pathway structuring of the quartets within a collapsed compact coil-like ensemble (perhaps resembling the molten globule state in protein folding, Fig. 8). The coil ensemble sampled diverse guanine-guanine interactions and progressed toward the native G4 fold via multiple small incremental steps. Thus, the G4 structure emerged from the compact coil-like ensemble via numerous rearrangements. This is significantly different from previous literature folding models that proceeded via a few simple intermediates, such as the Hoogsteen triplex. With potential consequences for experimental measurements, we also showed that the coil-like ensemble had a smaller radius of gyration than the native G4 (Fig. 4), implying that Rg is not a suitable marker for following the G4 folding process.

Our study also demonstrated significant methodological limitations. The ST-metaD simulation predicted a high positive $\Delta G_{fold}$ of +17 kcal/mol for the fully folded G4 (Table 2). To the best of our knowledge, this is the largest free energy discrepancy reported for nucleic acids simulations to date. Therefore, enhanced sampling simulations of the $(GGGA)_3GGG$ G4 structure may serve as a vital benchmark for DNA force field development. The free energy discrepancy was probably a result of several force field imbalances, as discussed above. Fortunately, folded G4 molecules can be reliably studied by standard simulations since they represent deep free energy basins on the FES and are separated from the unfolded ensemble by large free energy barriers. Nevertheless, the present study suggests that the global force-field description of the G4 folding landscapes is severely imbalanced. Further studies are needed to understand the origin of the imbalances and determine how (and if) they can be corrected.

Despite using a sophisticated enhanced sampling protocol, the simulations remained far from rigorous convergence, which would require equivalent sampling in all demuxed (continuous) trajectories. This was

not achieved in either the full G4 sequence or hairpin simulations. Nevertheless, we suggest that the G4 folding events reported above provide valid insights into the mechanism of G4 folding.

In summary, we achieved complete folding of a full parallel G4 from an unfolded oligonucleotide and showed the prominent role of coil-like compacted ensembles. We suggest that ST-metaD and similar simulation protocols could be used in further studies of G4 folding mechanisms and metastable ensembles, although fully converged sampling of the G4 landscape is not yet within the reach of contemporary methods and computers. Finally, the current AMBER force fields were found to severely underestimate the stability of the folded parallel-stranded G4 with respect to the unfolded ensemble.

Supplementary data to this article can be found online at https://doi.org/10.1016/j.ijbiomac.2024.129712.

## Author statement

The authors did not use any AI or AI-assisted technology during the preparation of this work.

## Funding

This work was supported by the Czech Science Foundation [21–23718S].

## CRediT authorship contribution statement

**Pavlína Pokorná:** Data curation, Formal analysis, Investigation, Project administration, Writing – original draft, Writing – review & editing. **Vojtěch Mlýnský:** Formal analysis, Methodology, Writing – review & editing. **Giovanni Bussi:** Methodology, Writing – review & editing. **Jiří Šponer:** Conceptualization, Funding acquisition, Writing – review & editing. **Petr Stadlbauer:** Conceptualization, Project administration, Writing – review & editing.

## Declaration of competing interest

The authors declare that they have no known competing financial interests or personal relationships that could have appeared to influence the work reported in this paper.

## Data availability

Input files, stripped trajectory files (reactive trajectories and reference replicas for G4, reactive trajectories and reference replicas for selected hairpin simulations), bias files and the $\Delta G_{\text{fold}}$ calculation protocol are available on Zenodo (DOI: https://doi.org/10.5281/zenodo.8247280) and GitHub (www.github.com/sponerlab/G4_folding_parallel). PLUMED input files are available in the plumed-nest.org repository (plumID:23.033).

## Acknowledgements

We acknowledge computational resources provided by the Ministry of Education, Youth and Sports of the Czech Republic through e-INFRA CZ [ID:90254].

## References

[1] P. Murat, S. Balasubramanian, Existence and consequences of G-quadruplex structures in DNA, Curr. Opin. Genet. Dev. 25 (2014) 22–29, https://doi.org/10.1016/j.gde.2013.10.012.
[2] M.L. Bochman, K. Paeschke, V.A. Zakian, DNA secondary structures: stability and function of G-quadruplex structures, Nat. Rev. Genet. 13 (2012) 770–780, https://doi.org/10.1038/nrg3296.
[3] D. Varshney, J. Spiegel, K. Zyner, D. Tannahill, S. Balasubramanian, The regulation and functions of DNA and rna G-quadruplexes, Nat. Rev. Mol. Cell Biol. 21 (2020) 459–474, https://doi.org/10.1038/s41580-020-0236-x.
[4] J.L. Mergny, D. Sen, DNA quadruple helices in nanotechnology, Chem. Rev. 119 (2019) 6290–6325, https://doi.org/10.1021/acs.chemrev.8b00629.
[5] L. Stefan, D. Monchaud, Applications of guanine quartets in nanotechnology and chemical biology, Nat. Rev. Chem. 3 (2019) 650–668, https://doi.org/10.1038/s41570-019-0132-0.
[6] J. Dai, M. Carver, D. Yang, Polymorphism of human telomeric quadruplex structures, Biochim. 90 (2008) 1172–1183, https://doi.org/10.1016/j.biochi.2008.02.026.
[7] K.W. Lim, V.C.M. Ng, N. Martín-Pintado, B. Heddi, A.T. Phan, Structure of the human telomere in Na+ solution: an antiparallel (2+2) G-quadruplex scaffold reveals additional diversity, Nucleic Acids Res. 41 (2013) 10556–10562, https://doi.org/10.1093/nar/gkt771.
[8] S.A. Dvorkin, A.I. Karsisiotis, M. Webba da Silva, Encoding canonical DNA quadruplex structure, Sci. Adv. 4 (2018), https://doi.org/10.1126/sciadv.aat3007 eaat3007.
[9] P. Sengupta, A. Bhattacharya, G. Sa, T. Das, S. Chatterjee, Truncated G-quadruplex isomers cross-talk with the transcription factors to maintain homeostatic equilibria in c-myc transcription, Biochem. 58 (2019) 1975–1991, https://doi.org/10.1021/acs.biochem.9b00030.
[10] M. Webba da Silva, Geometric formalism for DNA quadruplex folding, Chem. - Eur. J. 13 (2007) 9738–9745, https://doi.org/10.1002/chem.200701255.
[11] P.A. Rachwal, T. Brown, K.R. Fox, Sequence effects of single base loops in intramolecular quadruplex DNA, FEBS Lett. 581 (2007) 1657–1660, https://doi.org/10.1016/j.febslet.2007.03.040.
[12] A. Bugaut, S. Balasubramanian, A sequence-independent study of the influence of short loop lengths on the stability and topology of intramolecular DNA G-quadruplexes, Biochem. 47 (2008) 689–697, https://doi.org/10.1021/bi701873c.
[13] J. Chen, M. Cheng, P. Stadlbauer, J. Šponer, J.-L. Mergny, H. Ju, J. Zhou, Exploring sequence space to design controllable G-quadruplex topology switches, CCS Chem. 4 (2022) 3036–3050, https://doi.org/10.31635/ccschem.021.202101357.
[14] A.Y.Q. Zhang, S. Balasubramanian, The kinetics and folding pathways of intramolecular G-quadruplex nucleic acids, J. Am. Chem. Soc. 134 (2012) 19297–19308, https://doi.org/10.1021/ja309851t.
[15] Y. Xue, J.Q. Liu, K.W. Zheng, Z.Y. Kan, Y.H. Hao, Z. Tan, Kinetic and thermodynamic control of G-quadruplex folding, Angew. Chem. Int. Ed. 50 (2011) 8046–8050, https://doi.org/10.1002/anie.201101759.
[16] R.D. Gray, J.O. Trent, J.B. Chaires, Folding and unfolding pathways of the human telomeric G-quadruplex, J. Mol. Biol. 426 (2014) 1629–1650, https://doi.org/10.1016/j.jmb.2014.01.009.
[17] J.T. Grün, H. Schwalbe, Folding dynamics of polymorphic G-quadruplex structures, Biopolymers 113 (2022) e23477, https://doi.org/10.1002/bip.23477.
[18] X. Long, M.D. Stone, Kinetic partitioning modulates human telomere DNA G-quadruplex structural polymorphism, PloS One 8 (2013) e83420, https://doi.org/10.1371/journal.pone.0083420.
[19] J. Šponer, G. Bussi, P. Stadlbauer, P. Kuhrová, P. Banáš, B. Islam, S. Haider, S. Neidle, M. Otyepka, Folding of guanine quadruplex molecules-funnel-like mechanism or kinetic partitioning? An overview from MD simulation studies, Biochim. Biophys. Acta Gen. Subj. 2017 (1861) 1246–1263, https://doi.org/10.1016/j.bbagen.2016.12.008.
[20] I. Bessi, H.R.A. Jonker, C. Richter, H. Schwalbe, Involvement of long-lived intermediate states in the complex folding pathway of the human telomeric G-quadruplex, Angew. Chem. Int. Ed. 54 (2015) 8444–8448, https://doi.org/10.1002/anie.201502286.
[21] J.Y. Lee, B. Okumus, D.S. Kim, T. Ha, Extreme conformational diversity in human telomeric DNA, Proc. Natl. Acad. Sci. 102 (2005) 18938–18943, https://doi.org/10.1073/pnas.0506144102.
[22] A. Marchand, V. Gabelica, Folding and misfolding pathways of G-quadruplex DNA, Nucleic Acids Res. 44 (2016) 10999–11012, https://doi.org/10.1093/nar/gkw970.
[23] M. Aznauryan, S. Sondergaard, S.L. Noer, B. Schiott, V. Birkedal, A direct view of the complex multi-pathway folding of telomeric G-quadruplexes, Nucleic Acids Res. 44 (2016) 11024–11032, https://doi.org/10.1093/nar/gkw1010.
[24] S.L. Noer, S. Preus, D. Gudnason, M. Aznauryan, J.L. Mergny, V. Birkedal, Folding dynamics and conformational heterogeneity of human telomeric G-quadruplex structures in Na+ solutions by single molecule fret microscopy, Nucleic Acids Res. 44 (2016) 464–471, https://doi.org/10.1093/nar/gkv1320.
[25] R. Štefl, T.E. Cheatham, N.A. Špačková, E. Fadrná, I. Berger, J. Koča, J. Šponer, Formation pathways of a guanine-quadruplex DNA revealed by molecular dynamics and thermodynamic analysis of the substates, Biophys. J. 85 (2003) 1787–1804, https://doi.org/10.1016/S0006-3495(03)74608-6.
[26] T. Mashimo, H. Yagi, Y. Sannohe, A. Rajendran, H. Sugiyama, Folding pathways of human telomeric type-1 and type-2 G-quadruplex structures, J. Am. Chem. Soc. 132 (2010) 14910–14918, https://doi.org/10.1021/ja105806u.
[27] W. Li, X.-M. Hou, P.-Y. Wang, X.-G. Xi, M. Li, Direct measurement of sequential folding pathway and energy landscape of human telomeric G-quadruplex structures, J. Am. Chem. Soc. 135 (2013) 6423–6426, https://doi.org/10.1021/ja4019176.
[28] V. Limongelli, S. De Tito, L. Cerofolini, M. Fragai, B. Pagano, R. Trotta, S. Cosconati, L. Marinelli, E. Novellino, I. Bertini, et al., The G-triplex DNA, Angew. Chem. Int. Ed. 52 (2013) 2269–2273, https://doi.org/10.1002/anie.201206522.
[29] Y. Bian, C. Tan, J. Wang, Y. Sheng, J. Zhang, W. Wang, Atomistic picture for the folding pathway of a hybrid-1 type human telomeric DNA G-quadruplex, PLoS Comput. Biol. 10 (2014) e1003562, https://doi.org/10.1371/journal.pcbi.1003562.
[30] L. Cerofolini, J. Amato, A. Giachetti, V. Limongelli, E. Novellino, M. Parrinello, M. Fragai, A. Randazzo, C. Luchinat, G-triplex structure and formation propensity,

Nucleic Acids Res. 42 (2014) 13393–13404, https://doi.org/10.1093/nar/gku1084.
[31] X.-M. Hou, Y.-B. Fu, W.-Q. Wu, L. Wang, F.-Y. Teng, P. Xie, P.-Y. Wang, X.-G. Xi, Involvement of G-triplex and G-hairpin in the multi-pathway folding of human telomeric G-quadruplex, Nucleic Acids Res. 45 (2017) 11401–11412, https://doi.org/10.1093/nar/gkx766.
[32] C. Yang, M. Kulkarni, M. Lim, Y. Pak, Insilico direct folding of thrombin-binding aptamer G-quadruplex at all-atom level, Nucleic Acid Res. 45 (2017) 12648–12656, https://doi.org/10.1093/nar/gkx1079.
[33] M. Havrila, P. Stadlbauer, P. Kührová, P. Banáš, J.-L. Mergny, M. Otyepka, J. Šponer, Structural dynamics of propeller loop: towards folding of RNA G-quadruplex, Nucleic Acids Res. 46 (2018) 8754–8771, https://doi.org/10.1093/nar/gky712.
[34] P. Stadlbauer, P. Kührová, L. Vicherek, P. Banáš, M. Otyepka, L. Trantírek, J. Šponer, Parallel G-triplexes and G-hairpins as potential transitory ensembles in the folding of parallel-stranded DNA G-quadruplexes, Nucleic Acids Res. 47 (2019) 7276–7293, https://doi.org/10.1093/nar/gkz610.
[35] R. Rocca, F. Palazzesi, J. Amato, G. Costa, F. Ortuso, B. Pagano, A. Randazzo, E. Novellino, S. Alcaro, F. Moraca, et al., Folding intermediate states of the parallel human telomeric G-quadruplex DNA explored using well-tempered metadynamics, Sci. Rep. 10 (2020) e3176, https://doi.org/10.1038/s41598-020-59774-x.
[36] P. Stadlbauer, L. Trantírek, T.E. Cheatham, J. Koča, J. Šponer, Triplex intermediates in folding of human telomeric quadruplexes probed by microsecond-scale molecular dynamics simulations, Biochim. 105 (2014) 22–35, https://doi.org/10.1016/j.biochi.2014.07.009.
[37] E. Kim, C. Yang, Y. Pak, Free-energy landscape of a thrombin-binding DNA aptamer in aqueous environment, J. Chem. Theory Comput. 8 (2012) 4845–4851, https://doi.org/10.1021/ct300714u.
[38] B. Islam, M. Sgobba, C. Laughton, M. Orozco, J. Šponer, S. Neidle, S. Haider, Conformational dynamics of the human propeller telomeric DNA quadruplex on a microsecond time scale, Nucleic Acids Res. 41 (2013) 2723–2735, https://doi.org/10.1093/nar/gks1331.
[39] P. Stadlbauer, P. Kuhrová, P. Banáš, J. Koča, G. Bussi, L. Trantírek, M. Otyepka, J. Šponer, Hairpins participating in folding of human telomeric sequence quadruplexes studied by standard and T-REMD simulations, Nucleic Acids Res. 43 (2015) 9626–9644, https://doi.org/10.1093/nar/gkv994.
[40] A.E. Bergues-Pupo, J.R. Arias-Gonzalez, M.C. Morón, A. Fiasconaro, F. Falo, Role of the central cations in the mechanical unfolding of DNA and RNA G-quadruplexes, Nucleic Acids Res. 43 (2015) 7638–7647, https://doi.org/10.1093/nar/gkv690.
[41] X. Zeng, L. Zhang, X. Xiao, Y. Jiang, Y. Guo, X. Yu, X. Pu, M. Li, Unfolding mechanism of thrombin-binding aptamer revealed by molecular dynamics simulation and Markov state model, Sci. Rep. 6 (2016) e24065, https://doi.org/10.1038/srep24065.
[42] D. Luo, Y. Mu, Computational insights into the stability and folding pathways of human telomeric DNA G-quadruplexes, J. Phys. Chem. B. 120 (2016) 4912–4926, https://doi.org/10.1021/acs.jpcb.6b01919.
[43] M. Kogut, C. Kleist, J. Czub, Molecular dynamics simulations reveal the balance of forces governing the formation of a guanine tetrad—a common structural unit of G-quadruplex DNA, Nucleic Acids Res. 44 (2016) 3020–3030, https://doi.org/10.1093/nar/gkw160.
[44] M. Gajarský, M.L. Živković, P. Stadlbauer, B. Pagano, R. Fiala, J. Amato, L. U. Tomáška, J. Šponer, J. Plavec, L. Trantírek, Structure of a stable G-hairpin, J. Am. Chem. Soc. 139 (2017) 3591–3594, https://doi.org/10.1021/jacs.6b10786.
[45] Y. Bian, W. Ren, F. Song, J. Yu, J. Wang, Exploration of the folding dynamics of human telomeric G-quadruplex with a hybrid atomistic structure-based model, J. Chem. Phys. 148 (2018) e204107, https://doi.org/10.1063/1.5028498.
[46] Y. Bian, F. Song, J. Zhang, J. Yu, J. Wang, W. Wang, Insights into the kinetic partitioning folding dynamics of the human telomeric G-quadruplex from molecular simulations and machine learning, J. Chem. Theory Comput. 16 (2020) 5936–5947, https://doi.org/10.1021/acs.jctc.0c00340.
[47] P. Stadlbauer, B. Islam, M. Otyepka, J. Chen, D. Monchaud, J. Zhou, J.-L. Mergny, J. Šponer, Insights into G-quadruplex–hemin dynamics using atomistic simulations: implications for reactivity and folding, J. Chem. Theory Comput. 17 (2021) 1883–1899, https://doi.org/10.1021/acs.jctc.0c01176.
[48] I. Kejnovská, P. Stadlbauer, L. Trantírek, D. Renčiuk, M. Gajarský, D. Krafčík, J. Palacký, K. Bednářová, J. Šponer, J.-L. Mergny, et al., G-quadruplex formation by DNA sequences deficient in guanines: Two tetrad parallel quadruplexes do not fold intramolecularly, Chem. - Eur. J. 27 (2021) 12115–12125, https://doi.org/10.1002/chem.202100895.
[49] Y. Bian, F. Song, Z. Cao, J. Yu, J. Wang, Structure-based simulations complemented by conventional all-atom simulations to provide new insights into the folding dynamics of human telomeric G-quadruplex, Chinese Phys. B. 30 (2021) e078702, https://doi.org/10.1088/1674-1056/abe1a7.
[50] L.L. Wang, R.A. Friesner, B.J. Berne, Replica exchange with solute scaling: a more efficient version of replica exchange with solute tempering (REST2), J. Phys. Chem. B 115 (2011) 9431–9438, https://doi.org/10.1021/jp204407d.
[51] A. Barducci, G. Bussi, M. Parrinello, Well-tempered metadynamics: a smoothly converging and tunable free-energy method, Phys. Rev. Lett. 100 (2008) e020603, https://doi.org/10.1103/PhysRevLett.100.020603.
[52] C. Camilloni, D. Provasi, G. Tiana, R.A. Broglia, Exploring the protein G helix free-energy surface by solute tempering metadynamics, Proteins: Struct., Funct., Bioinf. 71 (2008) 1647–1654, https://doi.org/10.1002/prot.21852.
[53] V. Mlynský, M. Janeček, P. Kuhrová, T. Frohlking, M. Otyepka, G. Bussi, P. Banáš, J. Šponer, Toward convergence in folding simulations of RNA tetraloops: comparison of enhanced sampling techniques and effects of force field modifications, J. Chem. Theory Comput. 18 (2022) 2642–2656, https://doi.org/10.1021/acs.jctc.1c01222.
[54] M. Karplus, D.L. Weaver, Protein folding dynamics: the diffusion-collision model and experimental data., protein science: a publication of the protein, Protein Sci. 3 (1994) 650–668, https://doi.org/10.1002/pro.5560030413.
[55] S.-Q. Liu, X.-L. Ji, Y. Tao, D.-Y. Tan, K.-Q. Zhang, Y.-X. Fu, S.-Q. Liu, X.-L. Ji, Y. Tao, D.-Y. Tan, et al., Protein folding, binding and energy landscape: a synthesis, in: Protein Engineering, IntechOpen, 2012, pp. 207–252.
[56] D.A. Case, K. Belfon, I.Y. Ben-Shalom, S.R. Brozell, D.S. Cerutti, et al., AMBER 20 (Version 21) (2021) https://ambermd.org.
[57] M. Trajkovski, M.W. da Silva, J. Plavec, Unique structural features of interconverting monomeric and dimeric G-quadruplexes adopted by a sequence from the intron of the n-myc gene, J. Am. Chem. Soc. 134 (2012) 4132–4141, https://doi.org/10.1021/ja208483v.
[58] G.N. Parkinson, M.P.H. Lee, S. Neidle, Crystal structure of parallel quadruplexes from human telomeric DNA, Nature. 417 (2002) 876–880, https://doi.org/10.1038/nature755.
[59] K.N. Luu, A.T. Phan, V. Kuryavyi, L. Lacroix, D.J. Patel, Structure of the human telomere in K+ solution: an intramolecular (3 + 1) G-quadruplex scaffold, J. Am. Chem. Soc. 128 (2006) 9963–9970, https://doi.org/10.1021/ja062791w.
[60] W.D. Cornell, P. Cieplak, C.I. Bayly, I.R. Gould, K.M. Merz, D.M. Ferguson, D. C. Spellmeyer, T. Fox, J.W. Caldwell, P.A. Kollman, A 2nd generation force-field for the simulation of proteins, nucleic-acids, and organic-molecules, J. Am. Chem. Soc. 117 (1995) 5179–5197, https://doi.org/10.1021/ja00124a002.
[61] J.M. Wang, P. Cieplak, P.A. Kollman, How well does a restrained electrostatic potential (RESP) model perform in calculating conformational energies of organic and biological molecules? J. Comput. Chem. 21 (2000) 1049–1074, https://doi.org/10.1002/1096-987X(200009)21:12<1049::AID-JCC3>3.0.CO;2-F.
[62] A. Pérez, I. Marchan, D. Svozil, J. Šponer, T.E. Cheatham, C.A. Laughton, M. Orozco, Refinenement of the Amber force field for nucleic acids: improving the description of alpha/gamma conformers, Biophys. J. 92 (2007) 3817–3829, https://doi.org/10.1529/biophysj.106.097782.
[63] M. Krepl, M. Zgarbová, P. Stadlbauer, M. Otyepka, P. Banáš, J. Koča, T. E. Cheatham, P. Jurečka, J. Šponer, Reference simulations of noncanonical nucleic acids with different χ variants of the Amber force field: quadruplex DNA, quadruplex RNA and Z-DNA, J. Chem. Theory Comput. 8 (2012) 2506–2520, https://doi.org/10.1021/ct300275s.
[64] M. Zgarbová, F.J. Luque, J. Šponer, T.E. Cheatham 3rd, M. Otyepka, P. Jurečka, Toward improved description of DNA backbone: revisiting epsilon and zeta torsion force field parameters, J. Chem. Theory Comput. 9 (2013) 2339–2354, https://doi.org/10.1021/ct400154j.
[65] M. Zgarbová, J. Šponer, M. Otyepka, I.I.I. Thomas E. Cheatham, R. Galindo-Murillo, P. Jurečka, Refinement of the sugar–phosphate backbone torsion beta for Amber force fields improves the description of Z- and B-DNA, J. Chem. Theory Comput. 11 (2015) 5723–5736, https://doi.org/10.1021/acs.jctc.5b00716.
[66] M. Zgarbova, J. Šponer, P. Jurečka, Z-DNA as a touchstone for additive empirical force fields and a refinement of the alpha/gamma DNA torsions for Amber, J. Chem. Theory Comput. 17 (2021) 6292–6301, https://doi.org/10.1021/acs.jctc.1c00697.
[67] H.J.C. Berendsen, J.R. Grigera, T.P. Straatsma, The missing term in effective pair potentials, J. Phys. Chem. 91 (1987) 6269–6271, https://doi.org/10.1021/j100308a038.
[68] I.S. Joung, T.E. Cheatham, Molecular dynamics simulations of the dynamic and energetic properties of alkali and halide ions using water-model-specific ion parameters, J. Phys. Chem. B 113 (2009) 13279–13290, https://doi.org/10.1021/jp902584c.
[69] F.-Y. Dupradeau, D.A. Case, C. Yu, R. Jimenez, F.E. Romesberg, Differential solvation and tautomer stability of a model base pair within the minor and major grooves of DNA, J. Am. Chem. Soc. 127 (2005) 15612–15617, https://doi.org/10.1021/ja054607x.
[70] P. Kuhrová, R.B. Best, S. Bottaro, G. Bussi, J. Šponer, M. Otyepka, P. Banáš, Computer folding of RNA tetraloops: identification of key force field deficiencies, J. Chem. Theory Comput. 12 (2016) 4534–4548, https://doi.org/10.1021/acs.jctc.6b00300.
[71] P. Kuhrová, V. Mlýnský, M. Zgarbová, M. Krepl, G. Bussi, R.B. Best, M. Otyepka, J. Šponer, P. Banáš, Improving the performance of the Amber RNA force field by tuning the hydrogen-bonding interactions, J. Chem. Theory Comput. 15 (2019) 3288–3305, https://doi.org/10.1021/acs.jctc.8b00955.
[72] C.W. Hopkins, S. Le Grand, R.C. Walker, A.E. Roitberg, Long-time-step molecular dynamics through hydrogen mass repartitioning, J. Chem. Theory Comput. 11 (2015) 1864–1874, https://doi.org/10.1021/ct5010406.
[73] G. Bussi, D. Donadio, M. Parrinello, Canonical sampling through velocity rescaling, J. Chem. Phys. 126 (2007) e014101, https://doi.org/10.1063/1.2408420.
[74] S. Bottaro, F. Di Palma, G. Bussi, The role of nucleobase interactions in RNA structure and dynamics, Nucleic Acids Res. 42 (2014) 13306–13314, https://doi.org/10.1093/nar/gku972.
[75] M.J. Abraham, T. Murtola, R. Schulz, S. Páll, J.C. Smith, B. Hess, E. Lindahl, Gromacs: high performance molecular simulations through multi-level parallelism from laptops to supercomputers, SoftwareX 1-2 (2015) 19–25, https://doi.org/10.1016/j.softx.2015.06.001.
[76] G.A. Tribello, M. Bonomi, D. Branduardi, C. Camilloni, G. Bussi, Plumed 2: new feathers for an old bird, Comput. Phys. Commun. 185 (2014) 604–613, https://doi.org/10.1016/j.cpc.2013.09.018.
[77] C. Micheletti, A. Laio, M. Parrinello, Reconstructing the density of states by history-dependent metadynamics, Phys. Rev. Lett. 92 (2004) e170601, https://doi.org/10.1103/PhysRevLett.92.170601.

[78] S. Bottaro, G. Bussi, G. Pinamonti, S. Reißer, W. Boomsma, K. Lindorff-Larsen, Barnaba: software for analysis of nucleic acid structures and trajectories, RNA 25 (2019) 219–231, https://doi.org/10.1261/rna.067678.118.
[79] P. Banáš, A. Mládek, M. Otyepka, M. Zgarbová, P. Jurečka, D. Svozil, F. Lankaš, J. Šponer, Can we accurately describe the structure of adenine tracts in B-DNA? Reference quantum-chemical computations reveal overstabilization of stacking by molecular mechanics, J. Chem. Theory Comput. 8 (2012) 2448–2460, https://doi.org/10.1021/ct3001238.
[80] A.A. Chen, A.E. Garcia, High-resolution reversible folding of hyperstable RNA tetraloops using molecular dynamics simulations, Proc. Natl. Acad. Sci. U. S. A. 110 (2013) 16820–16825, https://doi.org/10.1073/pnas.1309392110.
[81] K. Liebl, M. Zacharias, Toward force fields with improved base stacking descriptions, J. Chem. Theory Comput. 19 (2023) 1529–1536, https://doi.org/10.1021/acs.jctc.2c01121.
[82] J.T. Grün, A. Blümler, I. Burkhart, J. Wirmer-Bartoschek, A. Heckel, H. Schwalbe, Unraveling the kinetics of spare-tire DNA G-quadruplex folding, J. Am. Chem. Soc. 143 (2021) 6185–6193, https://doi.org/10.1021/jacs.1c01089.
[83] D. Müller, I. Bessi, C. Richter, H. Schwalbe, The folding landscapes of human telomeric RNA and DNA G-quadruplexes are markedly different, Angew. Chem. Int. Ed. 133 (2021) 10990–10996, https://doi.org/10.1002/ange.202100280.
[84] J. Jana, K. Weisz, Thermodynamic stability of G-quadruplexes: impact of sequence and environment, Chem. Bio. Chem. 22 (2021) 2848–2856, https://doi.org/10.1002/cbic.202100127.
[85] M. Nishio, K. Tsukakoshi, K. Ikebukuro, G-quadruplex: flexible conformational changes by cations, pH, crowding and its applications to biosensing, Biosens. Bioelectron. 178 (2021) 113030, https://doi.org/10.1016/j.bios.2021.113030.
[86] L. Chen, J. Dickerhoff, S. Sakai, D. Yang, DNA G-quadruplex in human telomeres and oncogene promoters: structures, functions, and small molecule targeting, Acc. Chem. Res. 55 (2022) 2628–2646, https://doi.org/10.1021/acs.accounts.2c00337.
[87] K. Gkionis, H. Kruse, J.A. Platts, A. Mládek, J. Koča, J. Šponer, Ion binding to quadruplex DNA stems. Comparison of MM and QM descriptions reveals sizable polarization effects not included in contemporary simulations, J. Chem. Theory Comput. 10 (2014) 1326–1340, https://doi.org/10.1021/ct4009969.
[88] A.M. Salsbury, J.A. Lemkul, Molecular dynamics simulations of the c-kit1 promoter G-quadruplex: importance of electronic polarization on stability and cooperative ion binding, J. Phys. Chem. B 123 (2019) 148–159, https://doi.org/10.1021/acs.jpcb.8b11026.
[89] J.A. Lemkul, Same fold, different properties: polarizable molecular dynamics simulations of telomeric and TERRA G-quadruplexes, Nucleic Acids Res. 48 (2020) 561–575, https://doi.org/10.1093/nar/gkz1154.
[90] B. Islam, P. Stadlbauer, M. Krepl, J. Koča, S. Neidle, S. Haider, J. Šponer, Extended molecular dynamics of a c-kit promoter quadruplex, Nucleic Acids Res. 43 (2015) 8673–8693, https://doi.org/10.1093/nar/gkv785.
[91] O. Love, R. Galindo-Murillo, M. Zgarbová, J. Šponer, P. Jurečka, T.E.I. Cheatham, Assessing the current state of amber force field modifications for DNA—2023 edition, J. Chem. Theory Comput. 19 (2023) 4299–4307, https://doi.org/10.1021/acs.jctc.3c00233.
[92] G. Bussi, A. Laio, Using metadynamics to explore complex free-energy landscapes, Nat. Rev. Phys. 2 (2020) 200–212, https://doi.org/10.1038/s42254-020-0153-0.
[93] J.B. Chaires, W.L. Dean, H.T. Le, J.O. Trent, Hydrodynamic models of G-quadruplex structures, Methods Enzymol. 562 (2015) 287–304, https://doi.org/10.1016/bs.mie.2015.04.011.
[94] P. Stadlbauer, L. Mazzanti, T. Cragnolini, D.J. Wales, P. Derreumaux, S. Pasquali, J. Šponer, Coarse-grained simulations complemented by atomistic molecular dynamics provide new insights into folding and unfolding of human telomeric G-quadruplexes, J. Chem. Theory Comput. 12 (2016) 6077–6097, https://doi.org/10.1021/acs.jctc.6b00667.